9-2021

Coupled Inversion of Hydraulic and Self-Potential Data from Transient Outflow Experiments to Estimate Soil Petrophysical Properties

Jing Xie
Boise State University

Yian Cui
Central South University

Qifei Niu
Boise State University

Received: 16 April 2021 | Accepted: 20 July 2021

DOI: 10.1002/vzj2.20157

Vadose Zone Journal

ORIGINAL RESEARCH ARTICLE

Coupled inversion of hydraulic and self-potential data from transient outflow experiments to estimate soil petrophysical properties

Jing Xie[1,2] | **Yian Cui**[1] | **Qifei Niu**[2]

[1] School of Geosciences and Info-Physics, Central South Univ., Changsha, Hunan, China

[2] Dep. of Geosciences, Boise State Univ., Boise, ID 83725, USA

Correspondence
Qifei Niu, Dep. of Geosciences, Boise State Univ., Boise, ID 83725, USA.
Email: qifeiniu@boisestate.edu

Assigned to Associate Editor Fred Zhang.

Funding information
American Chemical Society Petroleum Research Fund, Grant/Award Number: 60925–DNI9

Abstract

Hydraulicproperties of soils could play an important role in affecting the partitioning of precipitation in the critical zone. In addition to traditional approaches, in the last two decades, many geophysical methods have been used to aid the hydrologic characterization and measurement of geological materials. In particular, the self-potential (SP) method shows great potential in these hydrogeophysical applications. The objective of this study is to evaluate whether the addition of SP data can improve the estimation of hydraulic properties of soils in an outflow experiment. A stochastic, coupled hydrogeophysical inversion was developed, in which the governing equations were solved using the finite volume method and the parameter estimation was conducted using a Bayesian approach associated with the Markov chain Monte Carlo technique. The results show that the addition of SP data in the inversion could reduce the uncertainty related to the estimated hydraulic parameters of soils and the length of the associated 95% confidence interval can be shortened by ~1/3. It is also shown that the electrical properties of soils at saturated and unsaturated conditions may also be estimated from the outflow experiment when SP data are available. Compared with hydraulic parameters, the accuracy of the estimated electrical properties is slightly lower. Among them, the saturated streaming potential coupling coefficient C_{sat} has the highest accuracy and lowest uncertainty since C_{sat} directly influences the magnitude of SP signals. The accuracy of other electrical parameters is lower than that of C_{sat} (and hydraulic parameters), and the associated uncertainty can be one order of magnitude larger.

1 | INTRODUCTION

The spatial variability of hydraulic properties in the subsurface could significantly affect the partitioning of precipitation in the critical zone (Takagi & Lin, 2011), an open system extending from the top of the canopy to the base of active groundwater (Giardino & Houser, 2015), thus influencing the amount, routing, and residence time of groundwater (Brooks et al., 2015). Many experimental methods have been proven effective in characterizing the hydraulic properties of earth materials in the critical zone, including field sampling and then testing in the laboratory (Wieting et al., 2017), field hydraulic tests (Libohova et al., 2018; Zhang et al., 2020), and geophysical tests (Holbrook et al., 2014). As an important

Abbreviations: AM, adaptive Metropolis; MCMC, Markov chain Monte Carlo; SP, self-potential.

portion of the critical zone, the vadose zone plays a paramount role in affecting the water chemistry and dynamics in the critical zone (Jin et al., 2011). In particular, hydraulic properties of the vadose zone such as soil water retention curve and unsaturated hydraulic conductivity regulate the amount of water stored in the soil and drained into fractured bedrock and streams (Hammond et al., 2019) and thus could be the dominating parameters influencing the hydraulic partitioning in the critical zones in, for example, mountainous western United States. In addition to critical zone hydrology, the hydraulic properties of unsaturated soils are also important in other disciplines such as agriculture engineering (Kirkham, 2014), geotechnical engineering (Lu, 2020), and environmental sciences (Leme & Miguel, 2018).

In general, hydraulic properties of unsaturated soils can be either estimated with pedotransfer functions (Wösten et al., 2001) or measured with laboratory or field hydraulic tests (Tarantino et al., 2009). Pedotransfer functions, which are usually developed based on statistical regression analysis or theoretical modeling, predict soil hydraulic properties from some easy-to-measure properties usually available from soil surveys (Aimrun & Amin, 2009; Bouma, 1989; Jaiswal et al., 2013; Patil & Singh, 2016). Despite their simplicity, pedotransfer functions may not perform well when the chemical composition, texture, and/or fabric of the soil exceed the calibration range (Patil & Singh, 2016). In the laboratory, the unsaturated soil properties can be accurately measured with some steady-state hydraulic experiments such as the constant flow method proposed in Lu et al. (2006). However, this type of test is usually time consuming, especially for fine materials with low hydraulic conductivity (Moebius et al., 2007; Šimůnek et al., 1998). In contrast, a transient flow test could produce large amounts of hydraulic data (e.g., pore water pressure and flow rate) within a short time period (Gribb, 1996; Wayllace & Lu, 2012). Unsaturated hydraulic properties of the sample can be estimated from these transient data by either analytical calculations (Li et al., 2009) or inversion. In such an inversion, the difference between the measured and simulated transient hydraulic responses is minimized (Latorre et al., 2015; Šimůnek et al., 1998) to recover the soil hydraulic properties. This inversion-based parameter estimation can be either deterministic (Šimůnek & van Genuchten, 1997) or stochastic (Thoma et al., 2014). Compared with steady-state tests, transient tests reduce the measurement time significantly, and thus they have been increasingly adopted in practice to determine the unsaturated hydraulic properties of various soils (Bahrami & Aghamir, 2020; Elliott & Price, 2020).

Recently, geophysical measurements have been used to aid the estimation of hydraulic properties and to monitor various hydrological processes in the subsurface (Binley et al., 2015). These hydrogeophysical applications are based on the observed correlations between hydrological and geophysical properties of porous media (Lesmes & Friedman, 2005), such as water content and dielectric constant (Topp et al., 1980), hydraulic conductivity and resistivity (Purvance & Andricevic, 2000), and hydraulic conductivity and imaginary conductivity (Weller et al., 2015). One of the most prominent geophysical methods in hydrological applications is the self-potential (SP) method, which measures the natural occurrence of electric fields on the ground surface (Allègre et al., 2010; Mboh et al., 2012). The dominant contribution to the SP signals in hydrological settings is the so-called streaming potential, which is generated by water flow in geological materials with charged mineral surfaces (Sill, 1983; Revil et al., 2002). In general, the measured streaming potential is influenced by the water flow rate, surface charge density, and effective electrical conductivity of the material. Due to the direct coupling between water flow and streaming potential, the SP method has been used in groundwater hydrology (Revil & Jardani, 2013), for example, to estimate the hydraulic conductivity and geometry of an aquifer (Darnet et al., 2003), to locate flow pathways and estimate the seepage velocity in dams and embankments (Bolève et al., 2009), and to monitor transpiration-induced water flows (Voytek et al., 2019) and rainwater infiltration processes (Doussan et al., 2002; Hu et al., 2020; Jougnot et al., 2015) in the vadose zone.

At saturated conditions, the streaming potential of porous media has been extensively studied (Ishido, 1989), and theoretical models are available to describe or predict the streaming potential coupling coefficient (Hunter et al., 2013), a parameter quantifying the streaming potential generated in a material under a given pressure gradient. For unsaturated porous media, many models have also been developed to describe the coupling coefficient; these unsaturated models are developed either by modifying the Helmholtz–Smoluchowski equation (Darnet & Marquis, 2004; Guichet et al., 2003; Perrier & Morat, 2000; Thanh et al., 2020) or by upscaling the effective excess charge defined at the pore scale (Jougnot et al., 2020; Revil et al., 2007). The upscaling of the effective excess charge can be done by the volume averaging approach (Linde et al., 2007) and flux averaging approach (Jougnot et al., 2012; Soldi et al., 2019). It should

Core Ideas

- Self-potential data can reduce the uncertainty of hydraulic parameter estimation.
- Soil electrical properties can be estimated from transient hydraulic and SP data.
- Stochastic coupled inversion is suitable for hydrogeophysical parameter estimation.

be noted that existing unsaturated coupling coefficient models may work for one type of soils but fail for a different soil type. For instance, the model developed in Linde et al. (2007) has been successfully applied to sand (Jougnot & Linde, 2013; Mboh et al., 2012), but it fails to describe the SP responses of other soils (Jougnot et al., 2012, 2020; Zhang et al., 2017).

Recently, the SP method has been used in the laboratory to monitor the transient water flow in soil column tests (Allègre et al., 2014; Jougnot & Linde, 2013; Linde et al., 2007; Mboh et al., 2012). Due to the advent of coupled hydrogeophysical inversion schemes (Hinnell et al., 2010), it becomes possible to recover the unsaturated hydraulic properties of soils from both hydraulic and SP data (Mboh et al., 2012; Younes et al., 2018). There are two potential yet unproven benefits of incorporating SP measurement in a transient outflow experiment. First, SP signals induced by water flow could help better constrain some hydraulic parameters (e.g., saturated hydraulic conductivity; Schwärzel et al., 2006) that usually have high uncertainty if inverted from transient hydraulic data alone. Second, in addition to hydraulic properties, the electrical properties of soils in both saturated and unsaturated conditions may also be estimated (Younes et al., 2018). Note that accurately measuring the electrical properties of unsaturated soils is a challenging task because special instruments are often required to maintain a stable unsaturated condition (Merritt et al., 2016; Wu et al., 2017). Considering that many outflow experiment systems have been equipped with SP monitoring electrodes (Allègre et al., 2014; Linde et al., 2007; Mboh et al., 2012), it is thus necessary to quantitatively evaluate whether the estimation of hydraulic and electrical properties will benefit from the incorporation of SP data.

The objective of this study is to conduct such an evaluation using hydraulic and SP monitoring data during outflow experiments. These data will be inverted in the Bayesian framework with the coupled hydrogeophysical inversion approach (Hinnell et al., 2010) to estimate the hydraulic and electrical properties of soils. In this paper, we first introduce the coupled forward modeling of water flow and streaming potential generation in saturated and unsaturated soils, followed by the stochastic, coupled inversion, which adopts the adaptive Metropolis (AM) algorithm to estimate model parameters as well as their uncertainties. Synthetic outflow experiments are conducted on sand and loam samples to produce time-series cumulative flow, water pressure, and SP data. These datasets are inverted to obtain the electrical and hydraulic properties of soils, which are then compared with the true values to evaluate the benefits of including SP data. The stochastic, coupled inversion is also performed on published experimental data. Discussions and major conclusions are presented at the end of the paper.

2 | FORWARD MODELING OF WATER FLOW AND STREAMING POTENTIAL

In this section, we describe the governing equations for one-dimensional water flow and streaming potential in saturated and unsaturated soils. Constitutive relationships describing hydraulic (water content and hydraulic conductivity) and electrical properties (electrical conductivity and streaming potential coupling coefficient) of soils under different pore water pressures or degrees of saturations are also introduced. In this study, the governing equations are solved numerically with the finite volume method, and the details of the calculation are also presented in this section.

2.1 | Water flow in saturated and unsaturated soils

Water flow in saturated and unsaturated soils can be described by the Richards equation (Richards, 1931). Under defined initial and boundary conditions, the transient hydraulic responses of the soil can be determined by solving the Richards equation (van Dam & Feddes, 2000). The variable to be solved can be either water content or pore water pressure (head). The Richards equation, which combines Darcy's law and mass conservation (Brunone et al, 2003; Namin & Boroomand, 2012), is a highly nonlinear partial differential equation (Caviedes-Voullième et al., 2013), expressed as

$$\frac{\partial \theta}{\partial t} - \nabla \cdot K \nabla h - \frac{\partial K}{\partial z} = 0 \tag{1}$$

where θ is the volumetric water content ($m^3\ m^{-3}$), h is the pore water pressure head (m), z is the vertical coordinate (positive upward, m), t is time (s), and K is the hydraulic conductivity ($m\ s^{-1}$). Note that both θ and K are not constant but functions of h, known as the soil water retention curve $\theta(h)$ and hydraulic conductivity function $K(h)$. In this study, we use the van Genuchten–Mualem models to describe $\theta(h)$ and $K(h)$, which can be expressed respectively as (Caviedes-Voullième et al., 2013; Mualem, 1976; van Genuchten, 1980)

$$\theta(h) = \begin{cases} \frac{\theta_s - \theta_r}{\left[1+(\alpha|h|)^n\right]^{1-\frac{1}{n}}} + \theta_r, & h \le 0 \\ \theta_s, & h > 0 \end{cases} \tag{2}$$

and

$$K(h) = \begin{cases} K_s S_e^{0.5}\left[1 - \left(1 - S_e^{\frac{n}{n-1}}\right)^{1-\frac{1}{n}}\right]^2, & h \le 0 \\ K_s, & h > 0 \end{cases} \tag{3}$$

where θ_s and θ_r denote the saturated and residual water content ($m^3\ m^{-3}$), respectively, K_s is the saturated hydraulic conductivity ($m\ s^{-1}$), n is a unitless parameter characterizing the shape of the curve $\theta(h)$ and is mainly influenced by the pore size distribution of the material, α is a fitting parameter interpreted as the inverse of the air-entry pressure (m^{-1}), and S_e is the effective saturation expressed as

$$S_e = \frac{\theta - \theta_r}{\theta_s - \theta_r} \tag{4}$$

2.2 | Streaming potential

In a streaming potential problem, the total electrical current density $\mathbf{j}$ in a porous medium can be expressed as the sum of the conductive current density $\mathbf{j_c}$ and streaming current density $\mathbf{j_s}$ (Sill, 1983):

$$\mathbf{j} = \mathbf{j_c} + \mathbf{j_s} \tag{5}$$

The conductive current density $\boldsymbol{j_c}$ is related to the electrical potential ϕ by Ohm's law:

$$\mathbf{j_c} = -\sigma \nabla \phi \tag{6}$$

where σ is the effective electrical conductivity of the medium (assumed to be isotropic, $S\ m^{-1}$). Applying the continuity condition (i.e., $\nabla \cdot \mathbf{j} = 0$) to Equation 5 results in the governing equation for the streaming potential:

$$\nabla \cdot (\sigma \nabla \phi) = \nabla \cdot \mathbf{j_s} \tag{7}$$

The effective electrical conductivity of porous geological media is influenced by many factors, including soil texture, water content, pore water chemistry, and mineral surface properties (Friedman, 2005). In this study, the empirical Archie's law is used to describe σ (Friedman, 2005):

$$\sigma = \frac{\sigma_w}{F} S^{n_a} + \sigma_s \tag{8}$$

where σ_w is the electrical conductivity of water ($S\ m^{-1}$), $F = \theta_s^{-m}$ is the formation factor (m being the porosity exponent or cementation exponent), $S = \theta/\theta_s$ is the degree of saturation, n_a is the Archie saturation exponent (Archie, 1942), and σ_s represents the surface conductivity ($S\ m^{-1}$; Revil & Glover, 1998). Equation 8 assumes that the surface conduction is in parallel with the conduction contributed from bulk water. Other more sophisticated electrical conductivity models (Bussian, 1983) may also be used here.

The streaming current density $\mathbf{j_s}$ can be explained by the electrokinetic theory (Ishido & Mizutani, 1981). In geological materials, the surface of minerals is usually charged, and ions in the pore water can accumulate near the solid–liquid interface in response to the charged mineral surface, forming the electrical double layer (EDL; Revil & Cerepi, 2004; Titov et al., 2005). The movement of water in the pore space will drag a portion of the excess charges in EDL, resulting in the streaming current (Revil & Jardani, 2013). In principle, the streaming current density in a porous medium is related to the amount of excess charge moving with water (i.e., the excess charge outside the shear plane; see Jougnot et al., 2020) and the velocity of the pore water (Leroy & Revil, 2004).

Considering a small length Δl of the material along the flow direction, the streaming current-induced electrical potential difference across this length $\Delta\phi$ can be determined using Ohm's law:

$$\Delta\phi = j_s \frac{\Delta l}{\sigma} \tag{9}$$

where j_s is the magnitude of the streaming current in the flow direction. The streaming potential coupling coefficient C is defined as the ratio of $\Delta\phi$ over the pressure increment ΔP across the length Δl driving the water flow [corresponding to the total head difference $\Delta(H_z + h)$ where H_z is the elevation head] (von Smoluchowski, 1903):

$$C = \frac{\Delta\phi}{\Delta\left(H_z + h\right)\rho_w g} \tag{10}$$

where ρ_w is the water density ($kg\ m^{-3}$) and g is the gravity acceleration ($m\ s^{-2}$).

Consider Darcy's law for the length Δl and then the Darcy velocity u in the flow direction can be expressed as

$$u = -K \frac{\Delta\left(H_z + h\right)}{\Delta l} \tag{11}$$

Inserting Equations 10 and 11 into Equation 9 yields the relationship between the streaming current density and Darcy velocity, which is expressed as (Linde et al., 2007 ; Revil et al., 2007; Younes et al., 2018)

$$j_s = -\rho_w g \frac{\sigma C}{K} u \tag{12}$$

If the Darcy velocity is treated as a vector (i.e., $\mathbf{u}$), the vector form of the streaming current density can be expressed as

$$\mathbf{j_s} = -\rho_w g \frac{\sigma C}{K} \mathbf{u} \tag{13}$$

Inserting Equation 13 into Equation 7 gives the governing equation for the streaming potential incorporating C:

$$\nabla \cdot (\sigma \nabla \phi) = \nabla \cdot \left(\rho_w g \frac{\sigma C}{K} \mathbf{u}\right) \tag{14}$$

It is noted that the parameters K and σ are dependent on the degrees of saturation (e.g., Equation 3 for K and Equation 8 for σ). The coupling coefficient C is also a function of saturation, and it can be linked to the coupling coefficient at saturation C_{sat}, for example, by (Linde et al., 2007)

$$C = \frac{C_{sat}}{S} \cdot \frac{K}{K_s} \cdot \frac{\sigma_{sat}}{\sigma} \tag{15}$$

where σ_{sat} is the effective electrical conductivity of the soil at saturation (i.e., Equation 8 with $S = 1$). Note that although Equation 15 has been successfully applied to sand (Jougnot & Linde, 2013), it may not work well for other types of soils (Zhang et al., 2017). Other constitutive models for C may be used (Perrier & Morat, 2000) to model the streaming potential in unsaturated soils when necessary.

2.3 | Finite volume method for the coupled forward modeling

For coupled water flow and streaming potential modeling, the governing equations include Equations 1 and 14 and the relevant constitutive models include Equations 2, 3, 8, and 15. Due to the highly nonlinear dependence of θ, K, σ, and C on h, analytical solutions of Equations 1 and 14 may only be available under some specific boundary conditions and simplified constitutive models (Namin & Boroomand, 2012). In general conditions, numerical methods are required to solve Equations 1 and 14 to determine the spatial and temporal distributions of h and ϕ in the soil. In this study, we use the finite volume method (Caviedes-Voullième et al., 2013; Eymard et al., 1999) to solve the governing equations, and many similar applications can be found in the literature (Manzini & Ferraris, 2004; Namin & Boroomand, 2012; Pei et al., 2006; Younes et al., 2018).

In our finite volume modeling, the sample domain is evenly divided into $N-1$ layers (with a thickness of Δz) by N notes. Define the pressure head and water content at node i ($i = 1, \ldots, N$) as θ_i and h_i, and then the discretized Equation 1 at time t reads

$$\frac{\partial \theta_i}{\partial t} = \frac{1}{\Delta z^2}\left[K_{i+1/2}\left(h_{i+1}-h_i\right) - K_{i-1/2}\left(h_i - h_{i-1}\right)\right] + \frac{1}{\Delta z}\left(K_{i+1/2} - K_{i-1/2}\right) \tag{16}$$

where $K_{i+1/2}$ (or $K_{i-1/2}$) represents the interlayer hydraulic conductivity between layer i and $i+1$ (or $i-1$). The interlayer conductivity can be calculated as the arithmetic mean, geometric mean, harmonic mean, or upstream mean of adjacent two layers (Baker, 2006; Caviedes-Voullième et al., 2013; Pei et al., 2006; Warrick, 1991). In general, when the hydraulic conductivity does not change significantly between adjacent layers, the simple arithmetic mean should be sufficient; otherwise, the other methods may be used to ensure numerical accuracy. In this study, the arithmetic mean was adopted [i.e., $K_{i+1/2} = (K_{i+1}+K_i)/2$ and $K_{i-1/2} = (K_{i-1}+K_i)/2$]. Similarly, define the electrical conductivity and electrical potential at node i as σ_i and ϕ_i and parameter $\delta = (\rho_w g \sigma C)/K$ at node i as $\delta_i = (\rho_w g \sigma_i C_i)/K_i$. The discretized Equation 14 can then be written as

$$\sigma_{i+1/2}\frac{\phi_{i+1}-\phi_i}{\Delta z} - \sigma_{i-\frac{1}{2}}\frac{\phi_i - \phi_{i-1}}{\Delta z} = \delta_{i+1/2}\, u_{i+1/2} - \delta_{i-1/2} u_{i-1/2} \tag{17}$$

where $\sigma_{i+1/2}$ (or $\sigma_{i-1/2}$) is the interlayer electrical conductivity between layers i and $i+1$ (or $i-1$) and $\delta_{i+1/2}$ (or $\delta_{i-1/2}$) is the average δ of two adjacent layers i and $i+1$ (or $i-1$). In this study, the arithmetic mean is used to calculate $\sigma_{i+1/2}$ (or $\sigma_{i-1/2}$).

The time domain to be solved can be divided into $M-1$ steps with increment Δt^j where $j = 1, \ldots, M$. The time step Δt^j may vary, and in this study, we use the implicit scheme in Caviedes-Voullième et al. (2013) to ensure that the solutions are accurate at large time steps. The discretized Equation 1 in the time domain can be expressed as (Caviedes-Voullième et al., 2013; Kumar, 1996)

$$\frac{\theta_i^{j+1}-\theta_i^j}{\Delta t^j} = \frac{1}{\Delta z^2}\left[K_{i+\frac{1}{2}}^{j+\frac{1}{2}}\left(h_{i+1}^{j+1}-h_i^{j+1}\right) - K_{i-\frac{1}{2}}^{j+\frac{1}{2}}\left(h_i^{j+1}-h_{i-1}^{j+1}\right)\right] + \frac{1}{\Delta z}\left(K_{i+1/2}^{j+1/2} - K_{i-1/2}^{j+1/2}\right) \tag{18}$$

where the index j indicates the associated variable at the time node j and the index $j+1/2$ indicates the average soil property during the time step Δt^j. In this study, the arithmetic mean is used to calculate the average K during a time increment. For Equation 14, temporal discretization is not needed, and Equation 17 will be solved after Equation 18 is solved at each time node. After the water content of the soil sample is calculated, the related cumulative outflow increment at the time node j (i.e., ΔQ^j) can then be determined by considering the average water content change of the sample. The cumulative outflow at time node j (i.e., Q^j) thus can be expressed as

$$Q^j = Q^{j-1} + A\sum_{i=1}^{N-1}\left(\theta_i^{j-1} - \theta_i^j\right)\Delta z \tag{19}$$

where A is the cross section area of the sample.

In the finite volume modeling of water flow, the following boundary conditions (Dirichlet and Neumann types) are applied (Allègre et al., 2010):

$$h(z,t) = h_b(t) \tag{20}$$

and

$$\left[-K(h)\frac{\partial h}{\partial z}-K(h)\right]_{i=1\text{or }N}=u_{\mathrm{b}}(t) \tag{21}$$

where $h_{\mathrm{b}}(t)$ and $u_b(t)$ are the pressure head and Darcy velocity at the boundaries. In streaming potential modeling, Dirichlet and Neumann type boundary conditions are also applied, expressed respectively as

$$\phi(z)=\phi_{\mathrm{b}} \tag{22}$$

and

$$\left[-\sigma\nabla\phi-\delta u\right]_{i\,=\,1\text{ or }N}=j_{\mathrm{b}} \tag{23}$$

where ϕ_{b} and j_{b} are the electrical potential and external current density at the boundary.

3 | STOCHASTIC COUPLED INVERSION

The hydraulic and geophysical properties of soils at saturated and unsaturated conditions can be estimated from the transient hydrogeophysical data using Bayesian inference, which uses probability distributions to describe model parameters **m**. Assume the prior information on the model parameters can be represented by the prior probability distributions $P_0(\mathbf{m})$. In Bayesian inference, the prior distributions $P_0(\mathbf{m})$ are updated as more information (e.g., measurement data **d**) becomes available, yielding the posterior probability distributions $\pi(\mathbf{m}|\mathbf{d})$ for the model parameters. From $\pi(\mathbf{m}|\mathbf{d})$, we can obtain not only a maximum likelihood model but also a quantification of the uncertainties of the model. Using Bayesian methods for parameter estimation has received increased popularity in many earth and environmental sciences such as atmosphere (Smith et al., 2009; Tamminen, 2004), geophysics (Grana et al., 2017; Ray & Myer, 2019), hydrology (Freni & Mannina, 2010; Tang et al., 2016), and environmental sciences (Ahmadi et al., 2015; Liu et al., 2021).

Due to the analytically intractable nature of many forward modeling problems, the implementation of the Bayesian method for parameter estimations is usually aided by the Markov chain Monte Carlo (MCMC) techniques, which use random walk approaches to generate samples that follow the posterior distributions of the model parameters (Vrugt et al., 2003). Over the years, many MCMC algorithms have been developed to sample the model space, including the Metropolis–Hastings algorithm (Hastings, 1970; Metropolis et al, 1953) and its variants such as the delayed rejection adaptive algorithm (Tierney & Mira, 1999). In this study, we adopted the AM algorithm (Haario et al., 2001) to sample the model parameters that characterize the hydraulic and electrical properties of soils under saturated and unsaturated conditions.

3.1 | Adaptive Metropolis algorithm

The AM algorithm is based on the conventional Metropolis algorithm with symmetric Gaussian proposal distributions, and during the MCMC sampling process, the sizes and orientations of the proposal distributions vary (Haario et al., 2001). The AM algorithm has the advantages of keeping detailed balance and ergodicity and showing great efficiency on complex and highly nonlinear target distributions (Saksman & Vihola, 2010; Tamminen, 2004). In practice, the AM algorithm can be realized with the following steps (Tamminen, 2004). Assume we have already sampled k model vectors $\mathbf{m}^0, \ldots, \mathbf{m}^{k-1}$. To get the next model vector $\mathbf{m}^k$, a candidate vector **Z** is sampled from the Gaussian proposal distribution with the mean value at the current point $\mathbf{m}^{k-1}$ and with the covariance matrix $\mathbf{C}^k$. The covariance matrix can be expressed as

$$\mathbf{C}^k=\begin{cases}\mathbf{C}^0, & k\le k_0\\ s_n\mathbf{K}^k+s_n\varepsilon I, & k>k_0\end{cases} \tag{24}$$

where $\mathbf{K}^k=\mathrm{cov}\,(\mathbf{m}^0,\ldots,\mathbf{m}^{k-1})$, $s_n=(2.4)^2/n$ is a scaling parameter (n being the dimension of the vector **Z**), ε is a small value (e.g., 10^{-10}) to prevent $\mathbf{C}^k$ from being singular, **I** is an $n\times n$ identity matrix, and k_0 defines the burn-in period, during which, the covariance matrix $\mathbf{C}^k$ is not updated. The samples in the burn-in period will be discarded in the calculation of the posterior distributions such that the impact of initial point ($\mathbf{m}^0$) can be minimized (Tamminen, 2004).

In the next step, the sampled vector **Z** is either accepted (i.e., $\mathbf{m}^k=\mathbf{Z}$) or rejected (thus, $\mathbf{m}^k=\mathbf{m}^{k-1}$). The probability of accepting **Z** is

$$\beta\left(\mathbf{m}^{k-1},\mathbf{Z}\right)=\min\left[\frac{\pi(\mathbf{Z})}{\pi\left(\mathbf{m}^{k-1}\right)},\,1\right] \tag{25}$$

In the AM algorithm, the ratio $\pi(\mathbf{Z})/\pi(\mathbf{m}^{k-1})$ can be expressed as (Tamminen, 2004)

$$\frac{\pi(\mathbf{Z})}{\pi\left(\mathbf{m}^{k-1}\right)}=\frac{P_0(\mathbf{Z})\,P(\mathbf{d}|\,\mathbf{Z})}{P_0\left(\mathbf{m}^{k-1}\right)P\left(\mathbf{d}|\,\mathbf{m}^{k-1}\right)} \tag{26}$$

where the likelihood $P(\mathbf{d}|\mathbf{Z})$ [or $P(\mathbf{d}|\mathbf{m}^{k-1})$] is a measure of the degree of fit between observed data **d** and data predicted from forward modeling with parameters **Z** (or $\mathbf{m}^{k-1}$) (e.g., see Mosegaard & Tarantola, 1995) and the prior distribution $P_0(\mathbf{Z})$ [or $P_0(\mathbf{m}^{k-1})$] contains our existing knowledge of the model parameters. Thus, the computation of the acceptance

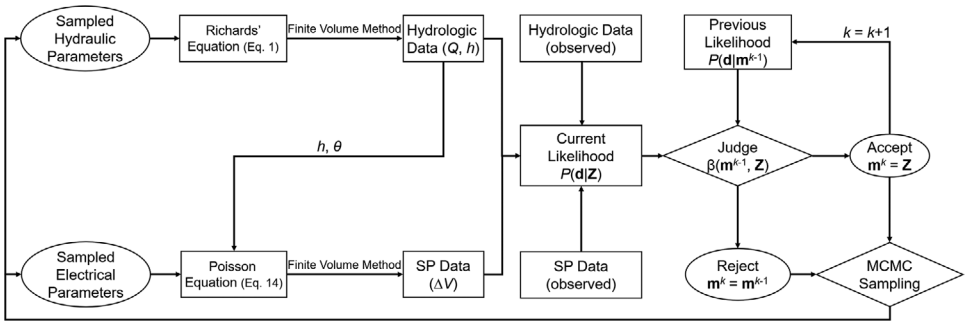

FIGURE 1 Flowchart of the coupled stochastic inversion using Markov chain Monte Carlo (MCMC) method. Q is the cumulative outflow; h is the pore water pressure head; θ is the volumetric water content; ΔV is the measured self-potential (SP); $\mathbf{m}^k$ and $\mathbf{m}^{k-1}$ are model vectors at step k and $k-1$, respectively; $\mathbf{Z}$ is a candidate vector; $P(\mathbf{d}|\mathbf{Z})$ [or $P(\mathbf{d}|\mathbf{m}^{k-1})$] is the likelihood measuring the degree of fit between observation $\mathbf{d}$ and $\mathbf{Z}$ (or $\mathbf{m}^{k-1}$); and $\beta(\mathbf{m}^{k-1}, \mathbf{Z})$ is the probability of accepting $\mathbf{Z}$

ratio involves mainly the evaluation of the likelihood. The above steps are iterated until k reaches a predefined number.

3.2 | MCMC inversion of transient hydrogeophysical data

In this study, the AM algorithm is used to obtain sample realizations of the model vector $\mathbf{m}$. The associated parameters include θ_r, α, n, $\log(K_s)$, m, n_a, and $C_{sat} \times 10^{-7}$. Using $\log(K_s)$ is to ensure the positivity of K_s in the inversion and multiplying C_{sat} by 10^{-7} will scale up the coupling coefficient to the same order of magnitude as the other parameters. Other parameters in the constitutive models such as θ_s and σ_w are relatively easy to determine in practice, and thus they are assumed known and will not be estimated in our inversion. The transient hydraulic data include the pore water pressure head h, cumulative outflow Q, and SP ϕ.

In this study, the hydraulic data and electrical data are inverted in a coupled way, which relies on the direct coupling between the streaming current $\mathbf{j}_s$ and Darcy velocity $\mathbf{u}$ (Equation 13) in the forward modeling and inversion process (Hinnell et al., 2010). The workflow of coupled hydrogeophysical inversions has been detailed in Ferré et al. (2009) and is also shown in Figure 1. In such a coupled inversion, an initial model is proposed, used to simulate transient responses based on coupled hydrologic and geophysical simulations (Equations 1 and 14), and then updated based on misfit between the simulated and observed transient data. In addition to the streaming current, the electrical conductivity of the soil is also dependent on the water content (e.g., Equation 8). In the inversion, both geophysical responses (ϕ) and hydraulic responses (Q and h) are used in quantifying the misfit between predicted and measured observations. Comparing to sequential inversion (Kang et al., 2020), the coupled inversion does not involve an intermediate geophysical inversion step before conducting the hydraulic inversion (or estimation), and thus it has the potential to reduce the uncertainties related to estimated hydrologic and geophysical properties and predicted hydraulic processes (Hinnell et al., 2010; Mboh et al., 2012).

In the MCMC inversion, it is usually assumed that the noise is additive and Gaussian, leading to the following likelihood function,

$$P(\mathbf{d}|\mathbf{Z}) \propto \exp\left(-\sum_{i=1}^{N_d} \frac{\sqrt{2}\,|f(\mathbf{Z}) - d_i|}{\varepsilon_i}\right) \tag{27}$$

where N_d is the total number of data points, f is a function denoting the forward modeling, and d_i and ε_i denote the ith data point and associated standard deviation, respectively. The l_1-norm is used in calculating the likelihood and it is less sensitive to outliers than the l_2-norm (Tarantola, 1987). It has been observed that most model parameters in this study [θ_r, α, n, $\log(K_s)$, m, n_a, and $C_{sat} \times 10^{-7}$] have limited ranges. For example, the cementation factor m of most geological materials ranges between 1 and 4 (Friedman, 2005). The prior knowledge of the bounds of model parameters can be easily incorporated in calculating the acceptance probability (Equation 25), expressed as

$$P_0(\mathbf{Z}) = \begin{cases} 1, & z \in [a, b] \\ 0, & \text{otherwise} \end{cases} \tag{28}$$

where $[a, b]$ is our predefined range for the model parameter z in $\mathbf{Z}$.

4 | SYNTHETIC EXPERIMENT AND INVERSION

In this section, the abovementioned stochastic coupled inversion is used to analyze the information content of transient hydraulic and SP data obtained from a typical outflow experiment. In particular, we will address the following two

TABLE 1 Synthetic soil samples and inversion scenarios considered in this study

Sample	Scenarios	Data used in inversion	Parameters to be inverted
Sand	Scenarios 1	Q, h	θ_r, α, n, K_s
	Scenarios 2	Q, h, and $\Delta\phi$	θ_r, α, n, K_s, n_a, C_{sat}, m
Loam	Scenarios 1	Q, h	θ_r, α, n, K_s
	Scenarios 2	Q, h, and $\Delta\phi$	θ_r, α, n, K_s, n_a, C_{sat}, m

Note: Q, cumulative outflow; h, pressure head; $\Delta\phi$, streaming potential difference; θ_r, residual water content; α, fitting parameter interpreted as the inverse of the air-entry pressure; n, the parameter characterizing the shape of the soil water retention curve; K_s, saturated hydraulic conductivity; n_a, the Archie saturation exponent; C_{sat}, the coupling coefficient at saturation; m, the porosity exponent.

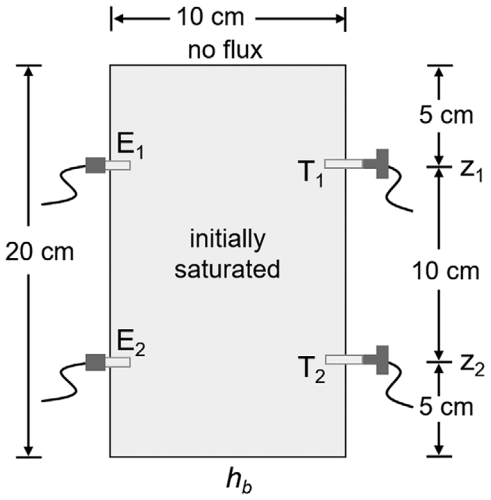

FIGURE 2 Schematic of a typical outflow experiment. Pore water pressure is measured at two depths using two tensiometers T_1 and T_2. Self-potential is measured at two depths using a pair of nonpolarizing electrodes E_1 and E_2. No flux is allowed at the upper boundary, and a pressure head h_b is applied to the initially saturated sample to drain the soil. z_1 and z_2 are different elevations

questions: (a) what is the uncertainty of the hydraulic and electrical properties estimated from transient hydrogeophysical data; and (b) to what degree will the addition of SP data reduce the uncertainty of the estimated hydraulic properties? Two synthetic soils are considered here (Table 1) for analysis.

4.1 | Synthetic outflow experiment

The schematic of a typical outflow experiment is shown in Figure 2. The soil sample is initially saturated, and a pressure head h_b is applied to the lower boundary to drain the soil sample. The ambient pressure on the upper boundary is equal to the atmospheric pressure but no flux is allowed. During the drainage process, the cumulative outflow Q is monitored. Electrical potential and pressure head are also monitored at two elevations z_1 and z_2 (Figure 2). This type of outflow experiments can be found, for example, in Allègre et al. (2014) and Linde et al. (2007). The measured transient data are used to estimate the hydraulic and electrical properties of the soil, including θ_r, α, n, K_s, m, n_a, and C_{sat}.

To test the accuracy of our forward modeling, we conducted an outflow simulation with a cylindrical soil sample (5 cm in radius and 20 cm in height; Figure 2). The sample is initially saturated and the total head is equal to 20 cm with datum at the base of the soil column. The applied h_b is -2 m. The cumulative outflow, pore water pressure head, and electrical potential during drainage were calculated using our numerical code. To facilitate the calculation, h_b was assumed to decrease linearly from 20 cm to -2 m in a short period (e.g., 100 s). The simulation was stopped when the cumulative outflow Q was not changing significantly. The following soil parameters were used in the simulation: $\theta_s = 0.3$ m^3 m^{-3}, $\theta_r = 0.03$ m^3 m^{-3}, $\alpha = 1.4$ m^{-1}, $n = 1.6$, $K_s = 5 \times 10^{-6}$ m s^{-1}, $n_a = 3.5$, $C_{sat} = -3.5 \times 10^{-7}$ V Pa^{-1}, $m = 2$, $\sigma_s = 0.002$ S m^{-1}, $\sigma_w = 0.1$ S m^{-1}, $\rho = 1{,}000$ kg m^{-3}, and $g = 10$ m s^{-2}. The electrical potential at the lower boundary is set as zero. The calculated hydraulic responses (h measured between T_1 and T_2) and electrical responses (potential difference $\Delta\phi$ measured between E_1 and E_2) are shown in Figure 3. To validate the accuracy of our calculation, the finite element method software COMSOL Multiphysics 5.6 (COMSOL) was also used to conduct the simulation and the results are shown in Figure 3. In general, the results from our numerical modeling are in good agreement with those from the COMSOL simulation. The related RMSDs of Q, h, and $\Delta\phi$ are 0.88 cm^3, 0.23 cm, and 0.0028 mV, respectively. This excellent agreement shows the effectiveness and accuracy of our numerical scheme in solving the coupled water flow and streaming potential problem.

4.2 | Sample 1: Sand

The first soil sample considered here is a sand with a porosity of 0.4. For the soil water retention curve, the van Genuchten model (Equation 2) is used and relevant parameters are $\alpha = 8$ m^{-1}, $\theta_s = 0.4$, $\theta_r = 0.01$, and $n = 5$; for the unsaturated hydraulic function, Equation 3 is used with $\log(K_s) = -4$ m s^{-1}. Archie's law incorporating the surface conduction (Equation 8) is used to model the effective electrical conductivity of

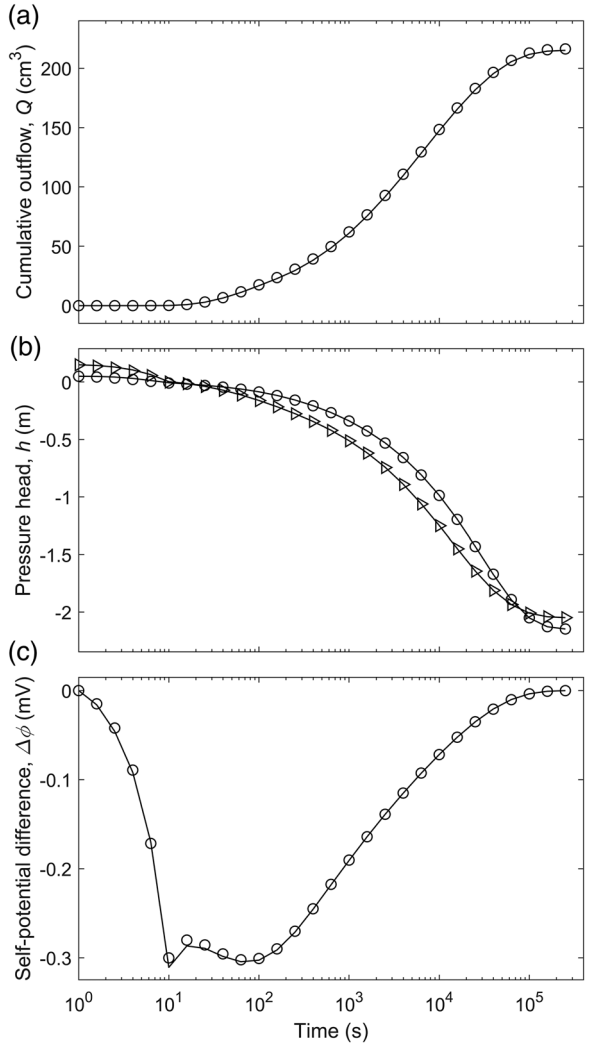

FIGURE 3 Transient hydraulic and electrical responses of a soil in an outflow experiment calculated with our numerical code (data points) and COMSOL Multiphysics (solid lines): (a) cumulative outflow Q; (b) pressure head h at two elevations (circles for z_1 and triangles for z_2); and (c) streaming potential difference $\Delta\phi$ between z_1 and z_2

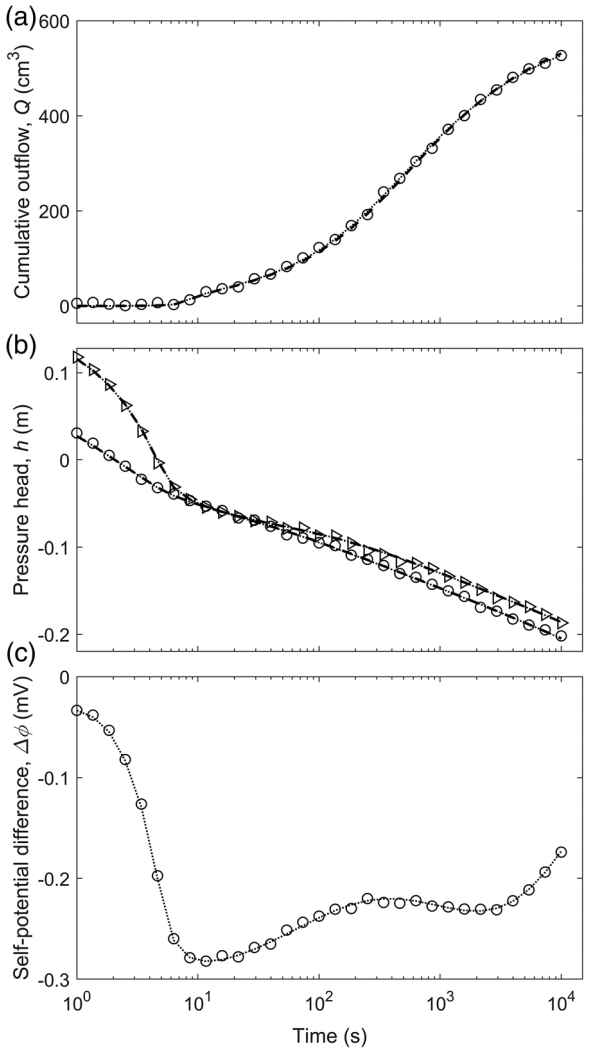

FIGURE 4 Hydraulic and electrical responses of a synthetic sand sample: (a) cumulative outflow Q; (b) pressure head h at two elevations (circles for z_1 and triangles for z_2); and (c) streaming potential difference $\Delta\phi$ between z_1 and z_2. Dashed and dotted lines represent the predictions calculated using the mean model parameters of Scenarios 1 and 2, respectively

the sand at various saturations with the following parameters: $n_a = 2.6$, $m = 1.6$, and $\sigma_s = 0.0002$ S m^{-1}. We use Equation 15 with $C_{sat} = -2.9 \times 10^{-7}$ V Pa^{-1} to model the streaming potential coupling coefficient of the sand with different degrees of saturation. These model parameters are summarized in Table 2. The sample is initially saturated and total head is 20 cm. In the outflow experiment, the pressure head at the lower boundary h_b was decreased from the initial value of 20 cm to −1 m within 30 s. The water pressure and electrical potential at z_1 and z_2 are monitored for 10^4 s as well as the cumulative outflow Q. These transient responses are shown in Figure 4.

Two scenarios were considered in our stochastic inversion (Table 1). In Scenario 1, only hydraulic data (i.e., Q and h at two elevations) are used in the inversion. The number of data points in each dataset is 30, and thus the total data points used in the inversion is 90. The measurement errors are set as 4 cm^3 and 0.2 cm respectively for Q and h. In the inversion, the parameter θ_s is fixed, considering the fact that the porosity of the sand sample is relatively easy to control or measure in the experiment. Initial values of θ_r, α, n, and $\log(K_s)$ are 0.015, 6 m^{-1}, 4, and −4.5 m s^{-1}, respectively, and the covariances are 0.005^2, 1.5^2, 1^2, and 0.2^2, respectively (also see Table 2). These initial values are selected as typical values of sandy samples (Schaap & Leij, 2000). These initial covariance values are chosen such that the sampling intervals of the proposal distributions (symmetric Gaussian) are approximately half of the predefined ranges of the model parameters (prior knowledge). The MCMC sampling is terminated after 30,000 runs and the chains of the sampled model parameters are shown

TABLE 2 Summary of the Markov chain Monte Carlo (MCMC) estimated model parameters for the synthetic sand sample

Parameter	True value	Prior mean (covariance)	Prior bounds	Inversion resultsof Scenario 1	Inversion resultsof Scenario 2
θ_r, $m^3\ m^{-3}$	0.01	0.015 (0.005^2)	0 ~ 0.05	**0.013** (30%) [0.009, 0.017] *61.5%*	**0.010** (0%) [0.009, 0.012] *30.0%*
α, m^{-1}	8.0	6.0 (1.5^2)	1 ~ 15	**8.04** (0.5%) [7.95, 8.13] *2.2%*	**8.00** (0%) [7.95, 8.04] *1.1%*
n	5.0	4.0 (1.0^2)	1.1 ~ 10	**4.97** (0.6%) [4.83, 5.11] *5.6%*	**5.03** (0.6%) [4.97, 5.08] *2.2%*
$\log(K_s)$, m s^{-1}	−4.0	−4.5 (0.2^2)	−5 ~ −3	**−3.99** (0.25%) [−4.00, −3.97] *0.8%*	**−4.00** (0%) [−4.01, −3.99] *0.5%*
n_a	2.6	2.0 (0.5^2)	1 ~ 5	–	**2.60** (0%) [2.58, 2.62] *1.5%*
$C_{sat} \times 10^{-7}$, V Pa^{-1}	−2.9	−3.5 (0.5^2)	−6 ~ −1	–	**−2.90** (0%) [−2.91, −2.88] *1.0%*
m	1.6	2.0 (0.2^2)	1 ~ 4	–	**1.60** (0%) [1.51, 1.68] *10.6%*

Note: In the fifth and sixth columns, the estimated mean values of model parameters are in bold, followed by the associated relative differences (in parentheses); the 95% confidence intervals (CIs) are included in square brackets, and the relative lengths of the 95% CIs are in italic. θ_r, residual water content; α, fitting parameter interpreted as the inverse of the air-entry pressure; *n*, the parameter characterizing the shape of the soil water retention curve; $\log(K_s)$, logarithm of saturated hydraulic conductivity; n_a, the Archie saturation exponent; C_{sat}, the coupling coefficient at saturation; *m*, the porosity exponent.

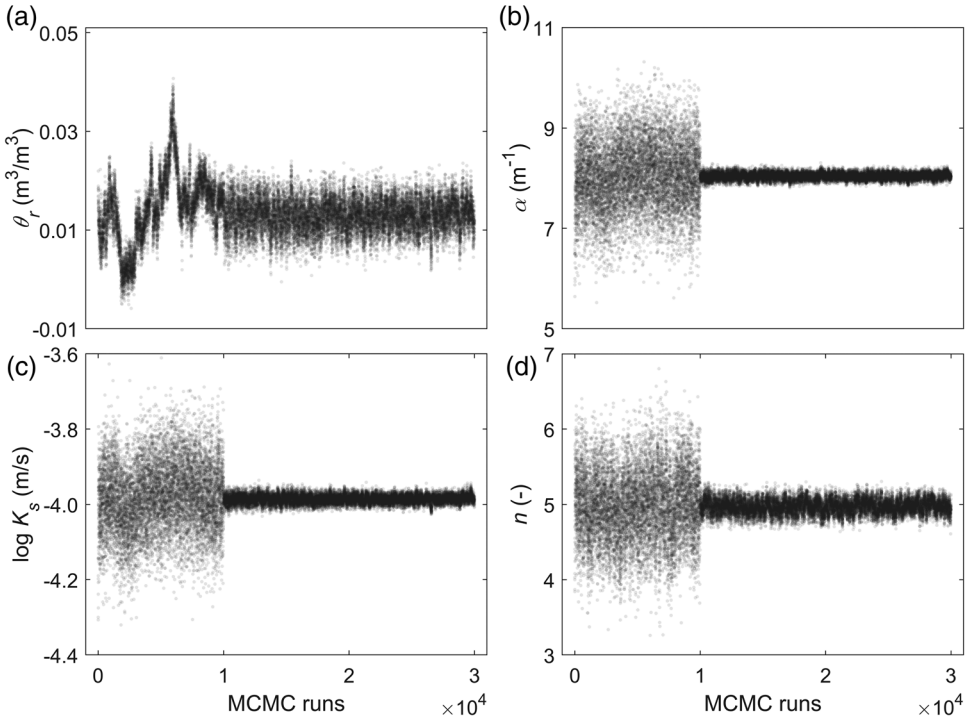

FIGURE 5 The sampled chains of the hydraulic properties of the synthetic sand sample (scenario 1): (a) θ_r, (b) α, (c) log K_s, and (d) *n*

in Figure 5. The first 10,000 runs are considered as the burn-in period, during which the covariances are not updated. The model parameters from the last 20,000 runs are used to estimate the statistical measures of the posterior distributions.

The MCMC estimated posterior distributions of the model parameters are shown in Figure 6 as histograms, which are calculated from the last 20,000 runs after the burn-in period. The mean value and 95% confidence interval (CI) of each parameter are estimated from the histograms and listed in Table 2. We also calculated the relative difference (i.e., absolute difference divided by the true value) between the estimated and true mean values as well as the relative length of the 95% CI (i.e., the length of the 95% CI normalized by the true value) for all the model parameters. In Table 2, it is apparent that the recovered model parameters are very close to the true values and the relative differences are generally less than ~1% except for θ_r, which also has a high uncertainty with a relative length of the 95% CI of ~61.5%. The model parameter $\log(K_s)$ has the lowest uncertainty with the length of the 95% CI as ~0.8% of its mean value. The results in Table 2 confirm that

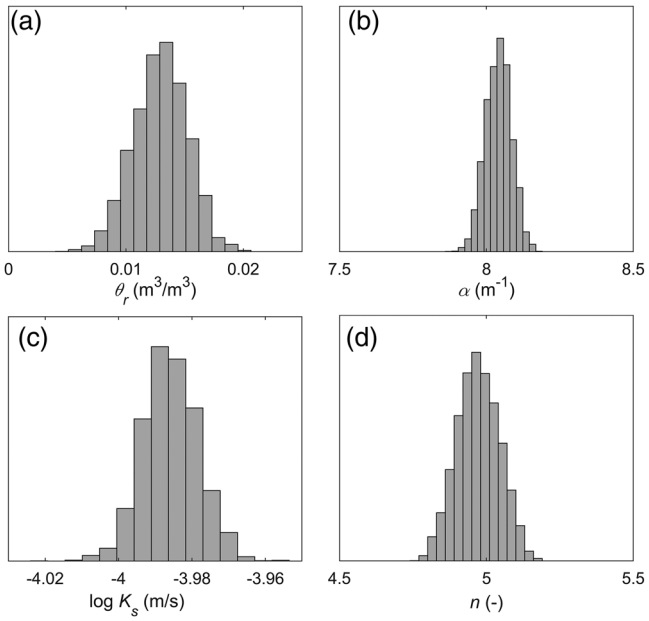

FIGURE 6 Markov chain Monte Carlo (MCMC)-estimated posterior distributions of the hydraulic properties of the sand sample (Scenario 1): (a) residual water content, θ_r; (b) fitting parameter interpreted as the inverse of the air-entry pressure, α; (c) logarithm of saturated hydraulic conductivity, log(K_s); and (d) the parameter characterizing the shape of the soil water retention curve, n

stochastic inversion can effectively recover the hydraulic properties of soils from the transient flow and pressure data.

The estimated mean values are used to calculate the transient hydraulic responses (Q and h) of the sand sample and the results (dashed lines) are shown in Figure 4. It is clear that the simulated Q and h agree very well with "measured" Q and h, and the related RMSDs are only 3.82 cm^3 and 0.19 cm. To evaluate the related prediction uncertainty, a couple of hundred sets of model parameters are drawn randomly from the posterior distributions in Figure 6 and are used to simulate the hydraulic responses. The variation ranges of the simulated Q and h are very narrow (not shown in Figure 4), generally smaller than the size of the data point symbols in Figure 4. Comparisons of experimental and simulated results in Figure 4 confirm that the transient outflow Q and pressure head h data in outflow experiments contain sufficient information on the saturated and unsaturated hydraulic properties of the sample (Toorman et al., 1992).

The second inversion (Scenario 2 in Table 1) is also conducted to estimate both the hydraulic and electrical properties of the sand sample from the "measured" outflow Q, water head h, and streaming potential difference Δϕ. The measurement errors of Q and h are same as those used in Scenario 1, and the error of SP measurements is set as 0.002 mV. In the inversion, the parameters θ_s and σ_w are considered known; σ_s is also assumed known, considering that the effect of surface conduction on SP signal is relatively small (Linde et al., 2007). The duration and time intervals of the monitoring data are the same as those used in Scenario 1. Parameters related to the MCMC sampling are also kept unchanged. The prior information on model parameters is summarized in Table 2 as well as the inversion results (mean values and 95% CIs). The inversion results are also shown in Figure 7 as histograms. The estimated mean values are used to simulate the hydraulic and geophysical responses during the drainage and the results are plotted in Figure 4 (dotted lines). Similar to Scenario 1, the agreement between the simulated and "measured" responses is excellent, and the related RMSDs for Q, Δϕ, and h are only 4.74 cm^3, 0.0026 mV, and 0.2 cm, respectively. We also evaluated the variation ranges of the predicted Q, Δϕ, and h responses (not shown in Figure 4); compared with Scenario 1, the calculated ranges of variations are quite similar though slightly narrower.

As shown in Table 2, both the recovered hydraulic and electrical parameters in Scenario 2 are very close to the true values. The associated uncertainties (i.e., relative length of the 95% CI) vary between 0.5% for log(K_s) and 30% for θ_r. Compared with Scenario 1, the estimated mean values in Scenario 2 are closer to the true values (Table 2); the related uncertainty (relative length of 95% CI) is also smaller, about half of those in Scenario 1. For example, the estimated mean n in Scenario 2 is 5.03 with the 95% CI as [4.97, 5.08], and the estimation from Scenario 1 is 4.97 with the 95% CI as [4.83, 5.11]; the relative length of 95% CI decreases from 5.6 to 2.2%. This indicates that the addition of transient SP data helps the estimation of hydraulic properties. Among the three electrical properties, the cementation factor m has the highest uncertainty, and the relative length of the 95% CI is ∼10.6%; in contrast, the values for C_{sat} and n_a are only ∼1 and 1.5%, respectively. This is consistent with the results shown in Younes et al. (2018). The relatively high uncertainty of m is understandable because, in such an outflow experiment (Figure 2), the effective electrical conductivity of the soil is not directly measured. On the contrary, the monitored SP signals are directly influenced by the coupling coefficient C_{sat}. Thus, m is less sensitive to the monitored transient data than C_{sat} (Younes et al., 2018).

4.3 | Sample 2: Loam

We also consider a loam sample to study if the soil texture affects the MCMC inversion results. Similarly, two scenarios are considered (i.e., inverting with Q and h, and with Q, h, and Δϕ; Table 1). Similarly, θ_s, σ_w, and σ_s are assumed known and the following constant values are used in the inversions: $\theta_s = 0.3$ m^3 m^{-3}, $\sigma_w = 0.1$ S m^{-1}, and $\sigma_s = 0.002$ S m^{-1}. Similar to the sand sample, the loam sample is initially saturated and the total head is 20 cm. In the forward modeling, a pressure head $h_b = -2$ m is gradually applied to the bottom within

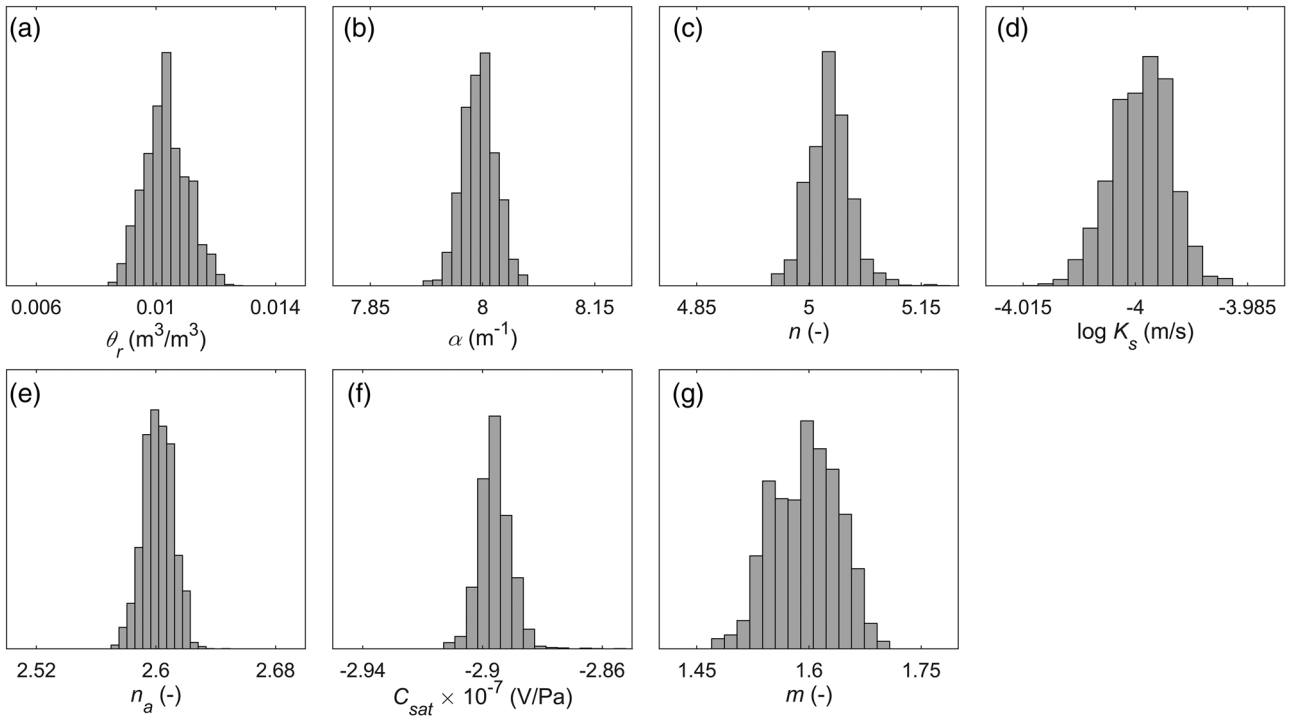

FIGURE 7 Markov chain Monte Carlo (MCMC)-estimated posterior distributions of the hydraulic and electrical properties of the synthetic sand sample (Scenario 2): (a) residual water content, θ_r; (b) fitting parameter interpreted as the inverse of the air-entry pressure, α; (c) the parameter characterizing the shape of the soil water retention curve, n; (d) logarithm of saturated hydraulic conductivity, log(K_s); (e) the Archie saturation exponent, n_a; (f) the coupling coefficient at saturation (C_{sat}) × 10^{-7}; and (g) the porosity exponent, m

150 s. The transient measurements available for the inversions begin at 1 s and end at 2×10^4 s after the onset of the outflow (see Figure 8). Other parameters are the same as those used in the sand sample.

The MCMC inversion results of the loam sample are summarized in Table 3. The transient hydraulic and electrical responses calculated using the MCMC estimated model parameters are shown in Figure 8. Similar conclusions can be made for the loam sample after analyzing the results: (a) using Q and h data are sufficient to accurately estimate the hydraulic properties of the sample; (b) addition of SP data can help reduce the uncertainty of the estimated hydraulic properties of the soil; and (c) the electrical properties of the sample can be estimated from Q, h, and Δϕ data with a fair accuracy, although not as well as hydraulic properties. In general, the lengths of the 95% CIs of the estimated hydraulic properties in Scenario 2 are about one- to two-thirds of those obtained in Scenario 1. Among all the hydraulic properties, θ_r has the highest uncertainty, and the relative length of the 95% CI is 96.6% for Scenario 1 and 62.1% for Scenario 2; log(K_s) has the lowest uncertainty, and the relative length of the 95% CI is lower than 2% for both scenarios. For the electrical properties, the estimation of C_{sat} is relatively accurate with the relative length of the 95% CI lower than 4%. In contrast, m and n_a have relatively high uncertainties and the relative length of the 95% CIs is higher than 50% (Table 3).

Comparison of results in Tables 2 and 3 indicates that the estimated model parameters are in general more accurate for the sand than the loam. For example, the relative length of the 95% CI for α is only 2.2% in Scenario 1 and 1.1% in Scenario 2 for the sand, but the values are 7.9 and 5% for the loam. The predicted electrical and hydraulic responses using the recovered model parameters (Figures 4 and 8) show similar trends, particularly for t larger than 100 s. The relatively better performance in sand is probably due to the fact that the transient data of sand used in inversions contain a larger portion of the drainage process (Kool et al., 1985). Note that the last portion of the cumulative outflow Q appears to approach a constant value for the sand (Figure 4), but it still has a tendency to increase for the loam (Figure 8). This implies that, to ensure a good performance on finer soils, the outflow experiment (Figure 2) should be performed for a longer period than coarse samples such that more information can be included in the measurement.

5 | INFLUENCE OF ELECTRICAL MODELS AND PARAMETERS

It has been found that the unsaturated streaming potential coupling coefficient C model (Equation 15) does not work for many soils (Jougnot et al., 2012, 2020; Zhang et al., 2017).

TABLE 3 Summary of the Markov chain Monte Carlo (MCMC) estimated model parameters for the synthetic loam sample

Parameter	True value	Prior mean and covariance	Prior bounds	Inversion results of Scenario 1	Inversion results of Scenario 2
θ_r, $m^3\ m^{-3}$	0.03	0.02 (0.006^2)	0 ~ 0.06	**0.029** (3.3%) [0.015, 0.043] *96.6%*	**0.029** (3.3%) [0.020, 0.038] *62.1%*
α, m^{-1}	1.4	1.8 (0.4^2)	0.01 ~ 4	**1.40** (0%) [1.34, 1.45] *7.9%*	**1.39** (0.7%) [1.36, 1.43] *5.0%*
n	1.6	2.0 (0.4^2)	1.01 ~ 4	**1.60** (0%) [1.55, 1.65] *6.3%*	**1.60** (0%) [1.58, 1.61] *1.9%*
$\log(K_s)$, $m\ s^{-1}$	−5.3	−5.0 (0.2^2)	−6.3 ~ −4.3	**−5.31** (0.2%) [−5.35, −5.26] *1.7%*	**−5.30** (0%) [−5.33, −5.28] *0.9%*
n_a	3.5	3.0 (0.5^2)	1 ~ 6	–	**3.57** (2%) [2.66, 4.48] *51.0%*
$C_{sat} \times 10^{-7}$, $V\ Pa^{-1}$	−3.5	−3.0 (0.5^2)	−7 ~ −1	–	**−3.53** (0.8%) [−3.59, −3.47] *3.4%*
m	2	2.5 (0.3^2)	1 ~ 4	–	**2.06** (3%) [1.39, 2.72] *64.6%*

Note: In the fifth and sixth columns, the estimated mean values of model parameters are in bold, followed by the associated relative differences (in parentheses); the 95% confidence intervals (CIs) are included in square brackets, and the relative lengths of the 95% CIs are in italic. θ_r, residual water content; α, fitting parameter interpreted as the inverse of the air-entry pressure; n, the parameter characterizing the shape of the soil water retention curve; $\log(K_s)$, logarithm of saturated hydraulic conductivity; n_a, the Archie saturation exponent; C_{sat}, the coupling coefficient at saturation; m, the porosity exponent.

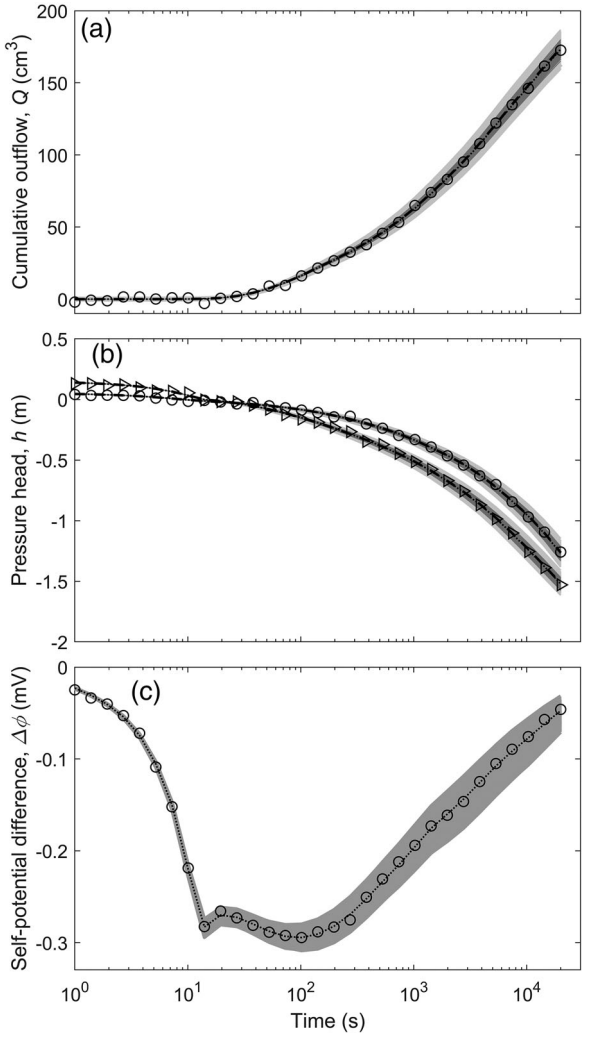

FIGURE 8 Hydraulic and electrical responses of the synthetic loam sample: (a) cumulative outflow Q; (b) pressure head h at two elevations (circles for z_1 and triangles for z_2); and (c) streaming potential difference $\Delta\phi$ between z_1 and z_2. Dashed and dotted lines represent the predictions calculated using the mean model parameters of Scenarios 1 and 2, respectively. The shaded regions represent the variation ranges of the prediction (light color for Scenario 1 and dark color for Scenario 2)

In addition, it is also difficult to accurately determine the surface conductivity σ_s (Equation 8) of a soil in practice. Thus, it is necessary to analyze how the unsaturated C models and an incorrect σ_s affect the coupled inversion.

5.1 | Influence of an incorrect σ_s

We invert the hydraulic and SP measurements of the loam sample once again with $\boldsymbol{\sigma_s} = 0$, and all the other parameters are kept unchanged. The inverted mean values of the model parameters are $\theta_r = 0.024\ m^3\ m^{-3}$, $\alpha = 1.37\ m^{-1}$, $n = 1.59$, $K_s = 10^{-5.32}\ m\ s^{-1}$, $n_a = 2.33$, $C_{sat} = -3.51$

TABLE 4 Summary of the Markov chain Monte Carlo (MCMC) estimated model parameters for the sand and loam samples with a different streaming potential coupling coefficient model (Equation 19)

Parameters	True values of sand sample	Inversion results of sand Scenario 2	True values of loam sample	Inversion results of loam Scenario 2
θ_r, $m^3\ m^{-3}$	0.01	**0.010** (0%) [0.007, 0.012] *50.0%*	0.03	**0.027** (10%) [0.024, 0.029] *18.5%*
α, m^{-1}	8.0	**8.03** (0.4%) [7.96, 8.08] *1.7%*	1.4	**1.40** (0%) [1.38, 1.42] *2.9%*
n	5.0	**5.03** (0.6%) [4.95, 5.14] *3.8%*	1.6	**1.60** (0%) [1.59, 1.61] *0.3%*
$\log(K_s)$, m s^{-1}	−4.0	**−3.99** (0.3%) [−4.00, −3.99] *0.3%*	–5.3	**−5.30** (0%) [−5.31, −5.28] *0.6%*
n_a	2.6	**2.58** (0.8%) [2.56, 2.60] *1.6%*	3.5	**3.47** (0.9%) [3.35, 3.63] *8.1%*
$C_{sat} \times 10^{-7}$, V Pa^{-1}	−2.9	**−2.90** (0%) [−2.91, −2.89] *0.7%*	–3.5	**−3.51** (0.3%) [−3.53, −3.49] *1.1%*
m	1.6	**1.56** (2.5%) [1.53, 1.60] *4.5%*	2	**2.00** (0%) [1.93, 2.09] *8.0%*

Note: In the third and fifth columns, the estimated mean values of model parameters are in bold, followed by the associated relative differences (in parentheses); the 95% confidence intervals (CIs) are included in square brackets, and the relative lengths of the 95% CIs are in italic. θ_r, residual water content; α, fitting parameter interpreted as the inverse of the air-entry pressure; n, the parameter characterizing the shape of the soil water retention curve; $\log(K_s)$, logarithm of saturated hydraulic conductivity; n_a, the Archie saturation exponent; C_{sat}, the coupling coefficient at saturation; m, the porosity exponent.

$\times 10^{-7}$ V Pa^{-1}, and $m = 1.63$. Compared with the inversion results with an accurate $\boldsymbol{\sigma_s}$ (Scenario 2 in Table 3), most of the recovered parameters are almost unchanged except n_a and m, which become noticeably smaller. According to Equation 8, a smaller n_a (or m) will increase the calculated electrical conductivity σ of the soil, which will compensate the effect of setting $\boldsymbol{\sigma_s} = 0$. This implies that using an incorrect σ_s in the coupled inversion only affects the other parameters appearing in the electrical conductivity model (Equation 8), and other model parameters are not influenced significantly.

5.2 | Influence of *C* models

In this subsection, we analyze if a different coupling coefficient model (other than Equation 15) will affect the conclusion made in our previous section. The unsaturated model proposed in Soldi et al. (2020) is used here, and it can be expressed as (see Equations 23 and 27 in Soldi et al., 2020)

$$C = C_{sat} S_e \frac{\sigma_{sat}}{\sigma} \tag{29}$$

The outflow experiments are simulated for both the sand and loam samples with the new C model and the measurements are then inverted to estimate the petrophysical properties of the samples. In the modeling and inversion, all the model parameters are kept unchanged. The inversion results are shown in Table 4.

In general, the recovered model parameters in Table 4 are very close to those in Tables 2 and 3. Both hydraulic properties and electrical properties of the samples are determined with a very small error. For the sand, the relative differences between estimated and true values range between 0 and 2.8%; for the loam, the related relative differences are between 0 and 10%. Compared with the results of Scenario 1 (Tables 2 and 3), the incorporation of SP data in the inversion with the new C model (Equation 29) also reduces the length of the 95% CIs significantly. For instance, the uncertainty of the parameter α (i.e., relative length of 95% CI) of the loam decreases from 7.9% in Scenario 1 in Table 3 to 2.9% in Table 4. Generally speaking, the inversion results associated with the new C model (Table 4) are consistent with those obtained with Equation 15. Therefore, the conclusions made in this study are still valid if other C models are used in the coupled inversion.

6 | INVERSION OF EXPERIMENTAL DATA

In this section, we apply the stochastic, coupled inversion to experimental data collected from an outflow test reported in Linde et al. (2007). The available datasets include transient Q, h, and ϕ measurements. The soil sample was cylindrical with a radius of 0.035 m and a height of 1.35 m. The sand was initially saturated and the saturated water content θ_s (or porosity) is between 0.33 and 0.35 (Linde et al., 2007). A pressure head $h_b = 0.091$ m was applied to the bottom to drain the sand column. During the drainage process, both h and ϕ were measured at a number of locations along the sand column. Some hydraulic and electrical properties of the sand have been independently measured (Linde et al., 2007, or summarized in Table 5): $\sigma_{sat} = 0.012$ S m^{-1}, $\sigma_w = 0.051$ S m^{-1}, $F = 4.26$, $C_{sat} = -2.9 \times 10^{-7}$ V Pa^{-1}, $K_s = 6.93 \times 10^{-5}$ m s^{-1}.

The datasets used in the inversion include ~1.8 h of cumulative outflow Q, ~4 h of pressure head h at two locations (22.5 and 47.5 cm from bottom), and ~4 h of SP ϕ at two locations (25 and 55 cm from bottom). In total, 30 data points were digitized from Linde et al. (2007) for Q and 40 for h and ϕ; the average time intervals of these data are between 200 and 1,000 s. Similar to synthetic soils, two inversion

TABLE 5 Summary of the Markov chain Monte Carlo (MCMC) estimated model parameters for the sand sample in Linde et al. (2007)

Parameters	Reference values (Linde et al., 2007)	Prior mean and covariance	Prior bounds	Inversion results of Scenario 1	Inversion results of Scenario 2
θ_s, $m^3\ m^{-3}$	0.33 ~ 0.35	0.3 (0.05^2)	0 ~ 0.7	**0.41** (20.6%) [0.34, 0.48] *34.2%*	**0.42** (23.5%) [0.35, 0.49] *33.3%*
α, m^{-1}	1.54	2.0 (0.2^2)	0.1 ~ 4	**1.40** (9.1%) [1.30, 1.50] *14.3%*	**1.38** (10.4%) [1.28, 1.48] *14.5%*
n	7.69	5.0 (1.0^2)	3 ~ 15	**7.45** (3.1%) [5.00, 9.91] *65.9%*	**7.18** (7.1%) [5.44, 8.91] *48.3%*
$\log(K_s)$, $m\ s^{-1}$	−4.16	−4.0 (0.15^2)	−5 ~ −3	**-4.17** (0.2%) [−4.19, −4.15] *1.0%*	**−4.17** (0.2%) [−4.18, −4.15] *0.7%*
n_a	1.6[a]	2.0 (0.15^2)	1 ~ 3	–	**1.75** (9.4%) [1.01, 2.49] *84.6%*
$C_{sat} \times 10^{-7}$, $V\ Pa^{-1}$	−2.9	−2.5 (0.4^2)	−6 ~ −1	–	**−3.42** (17.9%) [−3.57, −3.27] *8.8%*
m	1.30 ~ 1.38[b]	1.5 (0.15^2)	1 ~ 4	–	**1.28** (4.5%) [0.88, 1.69] *63.3%*

Note: In the fifth and sixth columns, the estimated mean values of model parameters are in bold, followed by the associated relative differences (in parentheses); the 95% confidence intervals (CIs) are included in square brackets, and the relative lengths of the 95% CIs are in italic.

[a]The value is not measured but assumed in Linde et al. (2007).

[b]It is calculated according to $F = \theta_s^{-m}$ with $F = 4.26$ and $\theta_s = 0.33$~0.35.

scenarios were considered (Table 5). In the inversions, the following model parameters were assumed known and thus kept unchanged: $\theta_r = 0.015\ m^3\ m^{-3}$, $\sigma_s = 0$, and $\sigma_w = 0.051\ S\ m^{-1}$. A total number of 8,000 runs were performed for the MCMC inversions, of which the first 4,000 runs were the burn-in period. The prior information on the model parameters is summarized in Table 5.

In Scenario 1, hydraulic parameters were inverted from Q and h and the results are summarized in Table 5. In general, the MCMC estimated mean values are close to the values reported in Linde et al. (2007). For α, n, and $\log(K_s)$, the relative differences are less than ~10%; for θ_s, the relative difference exceeds 20%. These discrepancies are probably due to the fact that h and ϕ data used in our inversion only cover ~4 h of the measurement. In contrast, the inversion in Linde et al. (2007) used transient h and ϕ data with a longer period that includes a free drainage stage (i.e., $h_b = 9.1$ cm was removed) in addition to the initial ~4 h. Despite these discrepancies, the modeled hydraulic responses using the MCMC estimated model parameters are very close to the measured responses (Figure 9). The associated RMSDs are only 0.9 cm^3 and 0.55 cm for Q and h, respectively. The good agreement in Figure 9 shows that the stochastic coupled inversion developed in this study could reliably estimate the hydraulic parameters of soils from transient hydraulic data collected in an outflow test.

The inversion results of Scenario 2 are also summarized in Table 5. Comparison of Scenarios 1 and 2 show that the estimated mean values of the hydraulic properties are very similar. The associated uncertainty (e.g., relative length of the 95% CI) is at the same level for parameters θ_s, α, n, and $\log(K_s)$. These results indicate that the addition of SP data may, although only slightly, reduce the uncertainty of the estimated hydraulic properties of the sand sample.

Regarding the electrical properties, it appears that the estimated mean values of n_a, C_{sat}, and m are close to the values reported in Linde et al. (2007), and the related relative differences are 9.4, 17.9, and 4.5%. Compared with hydraulic properties (e.g., results of Scenario 1), the discrepancies of electrical parameters between our estimations and reference values are slightly higher. It is also noted that the estimated 95% CIs (i.e., uncertainty) of the electrical parameters are quite large for n_a and m. Similar to synthetic soils, C_{sat} has the lowest uncertainty and the length of the 95% CI is only ~8.8% of the measured C_{sat}; this low uncertainty is because SP responses are directly affected by the streaming potential coupling coefficient of the soil (e.g., Equation 10). Moreover, the estimated m value (1.28 in Table 5) is lower than the typical value of unconsolidated sediments (Friedman, 2005). This is because, in the inversion, the surface conductivity was assumed zero (i.e., $\sigma_s = 0$; Linde et al., 2007). Assuming $\sigma_s = 0$ will overestimate the contribution of bulk water, thereby underestimating

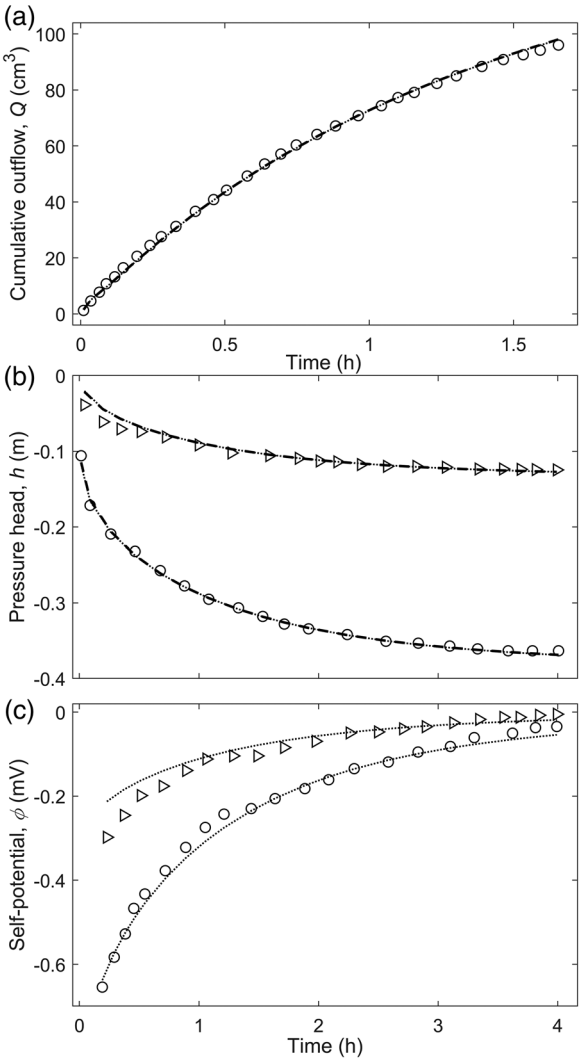

FIGURE 9 Hydraulic and electrical responses of the sand sample in Linde et al. (2007): (a) cumulative outflow Q; (b) pressure head h at two locations (circles for $z_1 = 47.5$ cm and triangles for $z_2 = 22.5$ cm); and (c) self-potential ϕ at two locations (circles for $z_1 = 55$ cm and triangles $z_2 = 25$ cm). Dashed and dotted lines represent the predictions calculated using the mean model parameters of Scenarios 1 and 2, respectively

the formation factor F and thus the value of m (Revil et al., 2015).

7 | CONCLUSIONS

In this study, stochastic, coupled inversions were performed to estimate hydraulic and electrical properties of soils from transient hydrogeophysical data collected in one-step outflow experiments. The time-series data used in the inversion include cumulative outflow Q, pressure head h, and/or SP ϕ. It is found that the stochastic inversion could provide information about the sensitivity of a soil's hydraulic and electrical properties to the measured Q, h, and ϕ in the outflow experiment. The results show that both saturated and unsaturated hydraulic properties of soils such as $\log(K_s)$, n, and α can be reliably estimated from transient Q and h data and the relative differences between estimation and true values are generally less than 10%. The accuracy of the estimated residual water content θ_r is much lower than other hydraulic properties, and the estimation is also associated with a larger uncertainty (the relative length of the 95% CI can reach ~100%). Comparison of the sand and loam samples indicates that the related uncertainty of the estimated hydraulic parameters can be reduced if the transient hydraulic data used in inversion cover a large portion of the drainage process.

Inversions including SP data were also performed. Compared with inversions with hydraulic data only (i.e., Q and h), the addition of SP data ϕ can reduce the uncertainty of the estimated hydraulic properties, although the mean value is not improved significantly. The related length of the 95% CIs for most hydraulic properties [e.g., $\log(K_s)$ and n] could be reduced by about one-third. This indicates that incorporating SP measurement in an outflow experiment is beneficial to the estimation of hydraulic properties. To the best of our knowledge, such a quantitative evaluation of the SP measurement in an outflow experiment was not available in the literature.

Inversion results also show that both saturated and unsaturated electrical properties (C_{sat}, n_a, and m) of the soil may be estimated from the hydraulic and SP data collected in outflow experiments. Among these electrical properties, the saturated streaming potential coupling coefficient C_{sat} has the highest accuracy and lowest uncertainty. The accuracy of other parameters such as m and n_a is slightly lower compared with C_{sat} (and hydraulic parameters). The associated uncertainty (relative length of the 95% CI) is generally large, about one order of magnitude higher than C_{sat} and hydraulic parameters (e.g., α and n). These different performances are due to the fact that parameters m and n_a do not directly affect the generation of streaming potential in an outflow experiment. In addition, it was also found that a good estimation of m and n relies on a correct surface conductivity value in the coupled inversion. The numerical findings in this study can serve as guidance in estimating soil petrophysical properties and their uncertainty from outflow experiments.

ACKNOWLEDGMENTS

Acknowledgment is made to the Donors of the American Chemical Society Petroleum Research Fund for partial support of this research. We thank three reviewers (Damien Jougnot and two anonymous reviewers) and the associate editor (Fred Zhang) for their constructive comments on an earlier version of this paper.

AUTHOR CONTRIBUTIONS

Jing Xie: Formal analysis; Investigation; Software; Validation; Visualization; Writing-original draft; Writing-review & editing. Yian Cui: Supervision; Writing-review & editing. Qifei Niu: Conceptualization; Formal analysis; Funding acquisition; Investigation; Methodology; Project administration; Resources; Supervision; Writing-review & editing.

CONFLICT OF INTEREST

The authors declare no conflict of interest.

ORCID

Qifei Niu https://orcid.org/0000-0003-2267-6653

REFERENCES

Ahmadi, A., Moridi, A., & Han, D. (2015). Uncertainty assessment in environmental risk through Bayesian networks. *Journal of Environmental Informatics*, *25*(1), 46–59. https://doi.org/10.3808/jei.201500294

Aimrun, W., & Amin, M. S. M. (2009). Pedo-transfer function for saturated hydraulic conductivity of lowland paddy soils. *Paddy Water Environ*, *7*, 217–225. https://doi.org/10.1007/s10333-009-0165-y

Allègre, V., Jouniaux, L., Lehmann, F., & Sailhac, P. (2010). Streaming potential dependence on water-content in Fontainebleau sand. *Geophysical Journal International*, *182*, 1248–1266. https://doi.org/10.1111/j.1365-246X.2010.04716.x

Allègre, V., Maineult, A., Lehmann, F., Lopes, F., & Zamora, M. (2014). Self-potential response to drainage-imbibition cycles. *Geophysical Journal International*, *197*, 1410–1424. https://doi.org/10.1093/gji/ggu055

Archie, G. E. (1942). The electrical resistivity log as an aid in determining some reservoir characteristics. *Transactions of the American Institute of Mining and Metallurgical Engineers*, *146*, 54–62.

Bahrami, A., & Aghamir, F. (2020). Simulation of vadose zone flow processes via inverse modeling of modified multistep outflow for fine-grained soils. *Soil Science Society of America Journal*, *84*(5), 1592–1605. https://doi.org/10.1002/saj2.20112

Baker, D. L. (2006). General validity of conductivity means in unsaturated flow models. *Journal of Hydrologic Engineering*, *11*(6), 526–538. https://doi.org/10.1061/(ASCE)1084-0699(2006)11:6(526)

Binley, A., Hubbard, S. S., Huisman, J. A., Revil, A., Robinson, D. A., Singha, K., & Slater, L. D. (2015). The emergence of hydrogeophysics for improved understanding of subsurface processes over multiple scales. *Water Resources Research*, *51*, 3837–3866. https://doi.org/10.1002/2015WR017016

Bolèkve, J., Revil, A., Janod, F., Mattiuzzo, J. L., & Fry, J.-J. (2009). Preferential fluid flow pathways in embankment dams imaged by self-potential tomography. *Near Surface Geophysics*, 447–462. https://doi.org/10.3997/1873-0604.2009012

Bouma, J. (1989). Using soil survey data for quantitative land evaluation. *Advances in Soil Science*, *9*, 177–213. https://doi.org/10.1007/978-1-4612-3532-3_4

Brooks, P. D., Chorover, J., Fan, Y., Godsey, S. E., Maxwell, R. M., Mcnamara, J. P., & Tague, C. (2015). Hydrological partitioning in the critical zone: Recent advances and opportunities for developing transferable understanding of water cycle dynamics. *Water Resources Research*, *51*(9), 6973–6987. https://doi.org/10.1002/2015WR017039

Brunone, B., Ferrante, M., Romano, N., & Santini, A. (2003). Numerical simulations of one-dimensional infiltration into layered soils with the Richards equation using different estimates of the interlayer conductivity. *Vadose Zone Journal*, *2*, 193–200. https://doi.org/10.2136/vzj2003.1930

Bussian, A. E. (1983). Electrical conductance in a porous medium. *Geophysics*, *48*(9), 1258–1268. https://doi.org/10.1190/1.1441549

Caviedes-Voullième, D., GarcıťA-Navarro, P., & Murillo, J. (2013). Verification, conservation, stability and efficiency of a finite volume method for the 1D Richards equation. *Journal of Hydrology*, *480*, 69–84. https://doi.org/10.1016/j.jhydrol.2012.12.008

Darnet, M., & Marquis, G. (2004). Modelling streaming potential (SP) signals induced by water movement in the vadose zone. *Journal of Hydrology*, *285*(1–4), 114–124. https://doi.org/10.1016/j.jhydrol.2003.08.010

Darnet, M., Marquis, G., & Sailhac, P. (2003). Estimating aquifer hydraulic properties from the inversion of surface streaming potential (SP) anomalies. *Geophysical Research Letters*, *30*(13), 1679. https://doi.org/10.1029/2003GL017631

Doussan, C., Jouniaux, L., & Thony, J.-L. (2002). Variations of self-potential and unsaturated water flow with time in sandy loam and clay loam soils. *Journal of Hydrology*, *267*(3–4), 173–185. https://doi.org/10.1016/S0022-1694(02)00148-8

Elliott, J., & Price, J. (2020). Comparison of soil hydraulic properties estimated from steady-state experiments and transient field observations through simulating soil moisture in regenerated Sphagnum moss. *Journal of Hydrology*, *582*, 124489. https://doi.org/10.1016/j.jhydrol.2019.124489

Eymard, R., Gutnic, M., & Hilhorst, D. (1999). The finite volume method for Richards equation. *Computational Geosciences*, *3*, 259–294. https://doi.org/10.1023/A:1011547513583

Ferré, T., Bentley, L., Binley, A., Linde, N., Kemna, A., Singha, K., Holliger, K., Huisman, J. A., & Minsley, B. (2009). Critical steps for the continuing advancement of hydrogeophysics. *Eos*, *90*(23), 200. https://doi.org/10.1029/2009EO230004

Freni, G., & Mannina, G. (2010). Bayesian approach for uncertainty quantification in water quality modelling: The influence of prior distribution. *Journal of Hydrology*, *392*, 31–39. https://doi.org/10.1016/j.jhydrol.2010.07.043

Friedman, S. P. (2005). Soil properties influencing apparent electrical conductivity: A review. *Computers and electronics in agriculture*, *46*(1–3), 45–70. https://doi.org/10.1016/j.compag.2004.11.001

Giardino, J. R., & Houser, C. (2015). Introduction to the critical zone. *Developments in Earth Surface Processes*, *19*, 1–13. https://doi.org/10.1016/B978-0-444-63369-9.00001-X

Grana, D., Fjeldstad, T., & Omre, H. (2017). Bayesian Gaussian mixture linear inversion for geophysical inverse problems. *Mathematical Geosciences*, *49*, 493–515. https://doi.org/10.1007/s11004-016-9671-9

Gribb, M. M. (1996). Parameter estimation for determining hydraulic properties of a fine sand from transient flow measurement. *Water Resources Research*, *32*(7), 1965–1974. https://doi.org/10.1029/96WR00894

Guichet, X., Jouniaux, L., & Pozzi, J.-P. (2003). Streaming potential of a sand column in partial saturation conditions. *Journal of Geophysical Research*, *108*(B3), 2141. https://doi.org/10.1029/2001JB001517

Haario, H., Saksman, E., & Tamminen, J. (2001). An adaptive Metropolis algorithm. *Bernoulli*, *7*, 223–242. https://doi.org/10.2307/3318737

Hammond, J. C., Harpold, A. A., Weiss, S., & Kampf, S. K. (2019). Partitioning snowmelt and rainfall in the critical zone: Effects of climate

type and soil properties. *Hydrology and Earth System Sciences*, *23*(9), 3553–3570. https://doi.org/10.5194/hess-23-3553-2019

Hastings, W. K. (1970). Monte Carlo sampling methods using Markov chains and their applications. *Biometrika*, *57*, 97–109. https://doi.org/10.1093/biomet/57.1.97

Hinnell, A. C., Ferré, T. P. A., Vrugt, J. A., Huisman, J. A., Moysey, S., Rings, J., & Kowalsky, M. B. (2010). Improved extraction of hydrologic information from geophysical data through coupled hydrogeophysical inversion. *Water Resources Research*, *46*, W00D40. https://doi.org/10.1029/2008WR007060

Holbrook, W. S., Riebe, C. S., Elwaseif, M. L., Hayes, J., Basler-Reeder, K. L., Harry, D., Malazian, A., Dosseto, A. C., Hartsough, P. W., & Hopmans, J. (2014). Geophysical constraints on deep weathering and water storage potential in the Southern Sierra Critical Zone Observatory. *Earth Surface Processes and Landforms*, *39*(3), 366–380. https://doi.org/10.1002/esp.3502

Hu, K., Jougnot, D., Huang, Q., Looms, M. C., & Linde, N. (2020). Advancing quantitative understanding of self-potential signatures in the critical zone through long-term monitoring. *Journal of Hydrology*, *585*, 124771. https://doi.org/10.1016/j.jhydrol.2020.124771

Hunter, R. J., Ottewill, R. H., & Rowell, R. L. (2013). *Zeta potential in colloid science: Principles and applications*. Elsevier Science.

Ishido, T. (1989). Self-potential generation by subsurface water flow through electrokinetic coupling. In G. P. Merkler, H. Militzer, H. Hötzl, H. Armbruster, & J. Brauns (Eds.) *Detection of subsurface flow phenomena* (Lecture Notes in Earth Sciences 27). Springer.

Ishido, T., & Mizutani, H. (1981). Experimental and theoretical basis of electrokinetic phenomena in rock-water systems and its applications to geophysics. *Journal of Geophysical Research: Solid Earth*, *86*(B3), 1763–1775. https://doi.org/10.1029/JB086iB03p01763

Jaiswal, R. K., Thomas, T., Galkate, R. V., & Jaivir, T. (2013). Soil water retention modeling using pedotransfer functions. *International Scholarly Research Notices*, *2013*, 208327. https://doi.org/10.1155/2013/208327

Jin, L., Andrews, D. M., Holmes, G. H., Lin, H., & Brantley, S. L. (2011). Opening the "black box": Water chemistry reveals hydrological controls on weathering in the Susquehanna Shale Hills Critical Zone Observatory. *Vadose Zone Journal*, *10*(3), 928–942. https://doi.org/10.2136/vzj2010.0133

Jougnot, D., & Linde, N. (2013). Self-potentials in partially saturated media: The importance of explicit modeling of electrode effects. *Vadose Zone Journal*, *12*(2). https://doi.org/10.2136/vzj2012.0169

Jougnot, D., Linde, N., Haarder, E. B., & Looms, M. C. (2015). Monitoring of saline tracer movement with vertically distributed self-potential measurements at the HOBE agricultural test site, Voulund, Denmark. *Journal of Hydrology*, *521*, 314–327. https://doi.org/10.1016/j.jhydrol.2014.11.041

Jougnot, D., Linde, N., Revil, A., & Doussan, C. (2012). Derivation of soil-specific streaming potential electrical parameters from hydrodynamic characteristics of partially saturated soils. *Vadose Zone Journal*, *11*(1). https://doi.org/10.2136/vzj2011.0086

Jougnot, D., Roubinet, D., Guarracino, L., & Maineult, A. (2020). Modeling streaming potential in porous and fractured media, description and benefits of the effective excess charge density approach. In A. Biswas & S. Sharma (Eds.), *Advances in modeling and interpretation in near surface geophysics* (pp. 61–96). Springer Geophysics. https://doi.org/10.1007/978-3-030-28909-6_4

Kang, X., Kokkinaki, A., Kitanidis, P. K., Shi, X., Revil, A., Lee, J., Soueid Ahmed, A., & Wu, J. (2020). Improved characterization of DNAPL source zones via sequential hydrogeophysical inversion of hydraulic-head, self-potential and partitioning tracer data. *Water Resources Research*, *56*(8), e2020WR027627. https://doi.org/10.1029/2020WR027627

Kirkham, M. B. (2014). *Principles of soil and plant water relations*. Academic Press.

Kool, J. B., Parker, J. C., & van Genuchten, M. Th. (1985). Determining soil hydraulic properties from one-step outflow experiments by parameter estimation: I. Theory and Numerical studies. *Soil Science Society of America Journal*, *49*(6), 1348–1354. https://doi.org/10.2136/sssaj1985.03615995004900060004x

Kumar, C. P. (1996). Prediction of evaporation losses from shallow water table using a numerical model. *Soil Water Flow*, *77*, 103–107.

Latorre, B., Peña, C., Lassabatere, L., Angulo-Jaramillo, R., & Moret-Fernández, D. (2015). Estimate of soil hydraulic properties from disc infiltrometer three-dimensional infiltration curve: Numerical analysis and field application. *Journal of Hydrology*, *57*, 1–12. https://doi.org/10.1016/j.jhydrol.2015.04.015

Leme, M. A. G., & Miguel, M. G. (2018). Permeability and retention to water and leachate of a compacted soil used as liner. *Water, Air, & Soil Pollution*, *229*, 374. https://doi.org/10.1007/s11270-018-4001-0

Leroy, P., & Revil, A. (2004). A triple-layer model of the surface electrochemical properties of clay minerals. *Journal of Colloid and Interface Science*, *270*, 371–380. https://doi.org/10.1016/j.jcis.2003.08.007

Lesmes, D. P., & Friedman, S. P. (2005). Relationships between the electrical and hydrogeological properties of rocks and soils. In Y. Rubin & S. S. Hubbard (Eds.), *Hydrogeophysics (pp.*. 87–128). Springer. https://doi.org/10.1007/1-4020-3102-5_4

Li, X., Zhang, L. M., & Fredlund, D. G. (2009). Wetting front advancing column test for measuring unsaturated hydraulic conductivity. *Canadian Geotechnical Journal*, *46*(12), 1431. https://doi.org/10.1139/T09-072

Libohova, Z., Schoeneberger, P., Bowling, L. C., Owens, P. R., Wysocki, D., Wills, S., Williams, C. O., & Seybold, C. (2018). Soil systems for upscaling saturated hydraulic conductivity for hydrological modeling in the critical zone. *Vadose Zone Journal*, *17*, 170051. https://doi.org/10.2136/vzj2017.03.0051

Linde, N., Jougnot, D., Revil, A., Matthäi, S. K., Arora, T., Renard, D., & Doussan, C. (2007). Streaming potential generation in two-phase flow conditions. *Geophysical Research Letters*, *34*, L03306. https://doi.org/10.1029/2006GL028878

Liu, J., Liu, R., Yang, Z., & Kuikka, S. (2021). Quantifying and predicting ecological and human health risks for binary heavy metal pollution accidents at the watershed scale using Bayesian Networks. *Environmental Pollution*, *269*, 116125. https://doi.org/10.1016/j.envpol.2020.116125

Lu, N. (2020). Unsaturated soil mechanics: Fundamental challenges, breakthroughs, and opportunities. *Journal of Geotechnical and Geoenvironmental Engineering*, *146*(5), 02520001. https://doi.org/10.1061/(ASCE)GT.1943-5606.0002233

Lu, N., Wayllace, A., Carrera, J., & Likos, W. J. (2006). Constant flow method for concurrently measuring soil–water characteristic curve and hydraulic conductivity function. *Geotechnical Testing Journal*, *29*(3), 1–12.

Manzini, G., & Ferraris, S. (2004). Mass-conservative finite volume methods on 2-D unstructured grids for the Richards' equation. *Advances in Water Resources*, *27*, 1199–1215. https://doi.org/10.1016/j.advwatres.2004.08.008

Mboh, C. M., Huisman, J. A., Zimmermann, E., & Vereecken, H. (2012). Coupled hydrogeophysical inversion of streaming potential signals

for unsaturated soil hydraulic properties. *Vadose Zone Journal*, *11*(2), vzj2011.0115. https://doi.org/10.2136/vzj2011.0115

Merritt, A. J., Chambers, J. E., Wilkinson, P. B., West, L. J., Murphy, W., Gunn, D., & Uhlemann, S. (2016). Measurement and modelling of moisture-electrical resistivity relationship of fine-grained unsaturated soils and electrical anisotropy. *Journal of Applied Geophysics*, *124*, 155–165. https://doi.org/10.1016/j.jappgeo.2015.11.005

Metropolis, N., Rosenbluth, A. W., Rosenbluth, M. N., Teller, A. H., & Teller, E. (1953). Equations of state calculations by fast computing machines. *The Journal of Chemical Physics*, *21*, 1087–1092. https://doi.org/10.1063/1.1699114

Moebius, B. N., Van Es, H. M., Schindelbeck, R. R., Idowu, O. J., Clune, D. J., & Thies, J. E. (2007). Evaluation of laboratory-measured soil properties as indicators of soil physical quality. *Soil Science*, *172*(11), 895–912. https://doi.org/10.1097/ss.0b013e318154b520

Mosegaard, K., & Tarantola, A. (1995). Monte Carlo sampling of solutions to inverse problems. *Journal of Geophysical Research*, *100*(B7), 12431–12447. https://doi.org/10.1029/94JB03097

Mualem, Y. (1976). A new model for predicting the hydraulic conductivity of unsaturated porous media. *Water Resources Research*, *12*(3), 513–522. https://doi.org/10.1029/WR012i003p00513

Namin, M. M., & Boroomand, M. R. (2012). A time splitting algorithm for numerical solution of Richard's equation. *Journal of Hydrology*, *444–445*, 10–21. https://doi.org/10.1016/j.jhydrol.2012.03.029

Patil, N. G., & Singh, S. K. (2016). Pedotransfer functions for estimating soil hydraulic properties: A review. *Pedosphere*, *26*(4), 417–430. https://doi.org/10.1016/S1002-0160(15)60054-6

Pei, Y., Wang, J., Tian, Z., & Yu, J. (2006). Analysis of interfacial error in saturated–unsaturated flow models. *Advances in Water Resources*, *29*, 515–524. https://doi.org/10.1016/j.advwatres.2005.06.007

Perrier, F., & Morat, P. (2000). Characterization of electrical daily variations induced by capillary flow in the non-saturated zone. *Pure and Applied Geophysics*, *157*, 785–810. https://doi.org/10.1007/PL00001118

Purvance, D. T., & Andricevic, R. (2000). Geoelectric characterization of the hydraulic conductivity field and its spatial structure at variable scales. *Water Resources Research*, *36*(10), 2915–2924. https://doi.org/10.1029/2000WR900187

Ray, A., & Myer, D. (2019). Bayesian geophysical inversion with trans-dimensional Gaussian process machine learning. *Geophysical Journal International*, *217*(3), 1706–1726. https://doi.org/10.1093/gji/ggz111

Revil, A., Binley, A., Mejus, L., & Kessouri, P. (2015). Predicting permeability from the characteristic relaxation time and intrinsic formation factor of complex conductivity spectra. *Water Resources Research*, *51*(8), 6672–6700. https://doi.org/10.1002/2015WR017074

Revil, A., & Cerepi, A. (2004). Streaming potentials in two-phase flow conditions. *Geophysical Research Letters*, *31*, L11605. https://doi.org/10.1029/2004GL020140

Revil, A., & Glover, P. W. J. (1998). Nature of surface electrical conductivity in natural sands, sandstones, and clays. *Geophysical Research Letters*, *25*(5), 691–694. https://doi.org/10.1029/98GL00296

Revil, A., Hermitte, D., Voltz, M., Moussa, R., Lacas, J.-G., Bourrié, G., & Trolard, F. (2002). Self-potential signals associated with variations of the hydraulic head during an infiltration experiment. *Geophysical Research Letters*, *29*(7), 1106. https://doi.org/10.1029/2001GL014294

Revil, A., & Jardani, A. (2013). *The self-potential method: Theory and applications in environmental geosciences*. Cambridge University Press.

Revil, A., Linde, N., Cerepi, A., Jougnot, D., Matthäi, S., & Finsterle, S. (2007). Electrokinetic coupling in unsaturated porous media. *Journal of Colloid and Interface Science*, *313*, 315–327. https://doi.org/10.1016/j.jcis.2007.03.037

Richards, L. A. (1931). Capillary conduction of liquids through porous mediums. *Physics*, *1*, 318–333. https://doi.org/10.1063/1.1745010

Rubin, Y., & Hubbard, S. S. (1996). *Hydrogeophysics*. Springer.

Saksman, E., & Vihola, M. (2010). On the ergodicity of the adaptive Metropolis algorithm on unbounded domains. *Annals of Applied Probability*, *20*(6), 2178–2203. https://doi.org/10.1214/10-AAP682

Schaap, M. G., & Leij, F. J. (2000). Improved prediction of unsaturated hydraulic conductivity with the Mualem-van Genuchten model. *Soil Science Society of America Journal*, *64*(3), 843–851. https://doi.org/10.2136/sssaj2000.643843x

Schwärzel, K., Šimůnek, J., Stoffregen, H., Wessolek, G., & van Genuchten, M. Th. (2006). Estimation of the unsaturated hydraulic conductivity of peat soils: Laboratory versus field data. *Vadose Zone Journal*, *5*(2), 628–640. https://doi.org/10.2136/vzj2005.0061

Sill, W. R. (1983). Self-potential modelling from primary flow. *Geophysics*, *48*, 76–86. https://doi.org/10.1190/1.1441409

Šimůnek, J., & van Genuchten, M. Th. (1997). Estimating unsaturated soil hydraulic properties from multiple tension disc infiltrometer data. *Soil Science*, *162*(6), 383–398. https://doi.org/10.1097/00010694-199706000-00001

Šimůnek, J., van Genuchten, M. Th., Gribb, M. M., & Hopmans, J. W. (1998). Parameter estimation of unsaturated soil hydraulic properties from transient flow processes. *Soil & Tillage Research*, *47*, 27–36.

Smith, R. L., Tebaldi, C., Nychka, D., & Mearns, L. O. (2009). Bayesian modeling of uncertainty in ensembles of climate models. *Journal of the American Statistical Association*, *104*(485), 97–116. https://doi.org/10.1198/jasa.2009.0007

Soldi, M., Guarracino, L., & Jougnot, D. (2020). An effective excess charge model to describe hysteresis effects on streaming potential. *Journal of Hydrology*, *588*, 124949. https://doi.org/10.1016/j.jhydrol.2020.124949

Soldi, M., Jougnot, D., & Guarracino, L. (2019). An analytical effective excess charge density model to predict the streaming potential generated by unsaturated flow. *Geophysical Journal International*, *216*(1), 380–394.

Takagi, K., & Lin, H. S. (2011). Temporal dynamics of soil moisture spatial variability in the Shale Hills Critical Zone Observatory. *Vadose Zone Journal*, *10*, 832–842. https://doi.org/10.2136/vzj2010.0134

Tamminen, J. (2004). Validation of nonlinear inverse algorithms with Markov chain Monte Carlo method. *Journal of Geophysical Research*, *109*, D19309. https://doi.org/10.1029/2004JD004927

Tang, Y., Marshall, L., Sharma, A., & Smith, T. (2016). Tools for investigating the prior distribution in Bayesian hydrology. *Journal of Hydrology*, *538*, 551–562. https://doi.org/10.1016/j.jhydrol.2016.04.032

A. Tarantino, E. Romero, & Y. Cui (Eds.). (2009). *Laboratory and field testing of unsaturated soils*. Springer.

Tarantola, A. (1987). Inversion of travel times and seismic waveforms. In G. Nolet (Ed.), *Seismic tomography: With applications in seismology and exploration geophysics* (pp. 135–157). Springer. https://doi.org/10.1007/978-94-009-3899-1_6

Thanh, L. D., Jougnot, D., Do, P. V., Ca, N. X., & Hien, N. T. (2020). A physically based model for the streaming potential coupling coefficient in partially saturated porous media. *Water*, *12*(6), 1588. https://doi.org/10.3390/w12061588

Thoma, M. J., Barrash, W., Cardiff, M., Bradford, J., & Mead, J. (2014). Estimating unsaturated hydraulic functions for coarse sediment from a field-scale infiltration experiment. *Vadose Zone Journal*, *13*(3). https://doi.org/10.2136/vzj2013.05.0096

Tierney, L., & Mira, A. (1999). Some adaptive Monte Carlo methods for Bayesian inference. *Statistics in Medicine*, *18*, 2507–2515. https://doi.org/10.1002/(SICI)1097-0258(19990915/30)18:17/18%3c2507::AID-SIM272%3e3.0.CO;2-J

Titov, K., Revil, A., Konosavsky, P., Straface, S., & Troisi, S. (2005). Numerical modelling of self-potential signals associated with a pumping test experiment. *Geophysical Journal International*, *162*, 641–650. https://doi.org/10.1111/j.1365-246X.2005.02676.x

Toorman, A. F., Wierenga, P. J., & Hills, R. G. (1992). Parameter estimation of hydraulic properties from one-step outflow data. *Water Resources Research*, *28*(11), 3021–3028. https://doi.org/10.1029/92WR01272

Topp, G. C., Davis, J. L., & Annan, A. P. (1980). Electromagnetic determination of soil water content: Measurements in coaxial transmission lines. *Water Resources Research*, *16*(3), 574–582. https://doi.org/10.1029/WR016i003p00574

van Dam, J. C., & Feddes, R. A. (2000). Numerical simulation of infiltration, evaporation and shallow groundwater levels with the Richards equation. *Journal of Hydrology*, *233*, 72–85. https://doi.org/10.1016/S0022-1694(00)00227-4

van Genuchten, M. Th. (1980). A closed-form equation for predicting the hydraulic conductivity of unsaturated soils. *Soil Science Society of America Journal*, *44*(5), 892–898. https://doi.org/10.2136/sssaj1980.03615995004400050002x

von Smoluchowski, M. (1903). Contribution to the theory of electro-osmosis and related phenomena. *Bulletin International de l'Academie des Sciences de Cracovie*, *3*, 184–199.

Voytek, E. B., Barnard, H. R., Jougnot, D., & Singha, K. (2019). Transpiration- and precipitation-induced subsurface water flow observed using the self-potential method. *Hydrological Processes*, *33*(13), 1784–1801.

Vrugt, J. A., Gupta, H. V., Bouten, W., & Sorooshian, S. (2003). A shuffled complex evolution Metropolis algorithm for optimization and uncertainty assessment of hydrologic model parameters. *Water Resources Research*, *39*(8), 1201. https://doi.org/10.1029/2002WR001642

Warrick, A. W. (1991). Numerical approximations of Darcian flow through unsaturated soil. *Water Resources Research*, *27*(6), 1215–1222. https://doi.org/10.1029/91WR00093

Wayllace, A., & Lu, N. (2012). A transient water release and imbibitions method for rapidly measuring wetting and drying soil water retention and hydraulic conductivity functions. *Geotechnical Testing Journal*, *35*(1), 103–117.

Weller, A., Slater, L., Binley, A., Nordsiek, S., & Xu, S. (2015). Permeability prediction based on induced polarization: Insights from measurements on sandstone and unconsolidated samples spanning a wide permeability range. *Geophysics*, *80*(2), 1MA–Z50. https://doi.org/10.1190/geo2014-0368.1

Wieting, C., Ebel, B. A., & Singha, K. (2017). Quantifying the effects of wildfire on changes in soil properties by surface burning of soils from the Boulder Creek Critical Zone Observatory. *Journal of Hydrology: Regional Studies*, *13*, 43–57. https://doi.org/10.1016/j.ejrh.2017.07.006

Wösten, J. H. M., Pachepsky, Y. A., & Rawls, W. J. (2001). Pedotransfer functions: Bridging the gap between available basic soil data and missing soil hydraulic characteristics. *Journal of Hydrology*, *251*(3–4), 123–150. https://doi.org/10.1016/S0022-1694(01)004-64-4

Wu, Y., Wang, Y. H., & Niu, Q. (2017). Integrating the four-probe method and SWCC device to measure electrical resistivity anisotropy of unsaturated soil. *Geotechnical Testing Journal*, *40*(4), 698–709. https://doi.org/10.1520/GTJ20160160

Younes, A., Zaouali, J., Lehmann, F., & Fahs, M. (2018). Sensitivity and identifiability of hydraulic and geophysical parameters from streaming potential signals in unsaturated porous media. *Hydrology and Earth System Sciences*, *22*, 3561–3574. https://doi.org/10.5194/hess-22-3561-2018

Zhang, J., Vinogradov, J., Leinov, E., & Jackson, M. D. (2017). Streaming potential during drainage and imbibition. *Journal of Geophysical Research: Solid Earth*, *122*(6), 4413–4435.

Zhang, X., Wendroth, O., Matocha, C., Zhu, J., & Reyes, J. (2020). Assessing field-scale variability of soil hydraulic conductivity at and near saturation. *Catena*, *187*, 104335. https://doi.org/10.1016/j.catena.2019.104335

How to cite this article: Xie J, Cui Y, & Niu Q. Coupled inversion of hydraulic and self-potential data from transient outflow experiments to estimate soil petrophysical properties. *Vadose Zone J*. 2021;*20:* e20157. https://doi.org/10.1002/vzj2.20157